NOVEL Bi_2MoO_6/g-C_3N_4 NANOCOMPOSITE FOR ENHANCED PHOTOCATALYTIC DEGRADATION OF METHYLENE BLUE DYE UNDER VISIBLE LED LIGHT IRRADIATION

Thesis Submitted

by

Snehashis Roy

Class Roll No.-002010402017

Examination Roll No.-M4CIV22017

Registration No.-153973 of 2020-2021

MASTER OF ENGINEERING

Under the supervision of

Prof. Ankush Majumdar

DEPARTMENT OF CIVIL ENGINERING
(ENVIRONMENTAL ENGINEERING DIVISION)
JADAVPUR UNIVERSITY
KOLKATA-700032, INDIA
2022

Declaration

*The Thesis titled "**Novel Bi_2MoO_6/g-C_3N_4 nanocomposite for enhanced photocatalytic degradation of methylene blue dye under visible LED light irradiation**" is prepared and submitted for the award of the degree of **Master of Engineering in Civil Engineering** course of **Jadavpur University** for the session of 2020-2022. I declare that the work described in this thesis is entirely my own. No portion of the work referred to in this thesis has been submitted in support of an application for another degree or qualification of this or any other university or institute. Any help or source information which has been awarded in the thesis, has been duly acknowledged.*

Snehashis Roy

Snehashis Roy

M.C.E- 2ND Yr.

Class Roll No- 002010402017

Examination Roll No- M4CIV22017

Registration No.-153973 of 2020-2021

Department of Civil Engineering

Environmental Engineering Division

Date: 27/06/2022

JADAVPUR UNIVERSITY
DEPARTMENT OF CIVIL ENGINEERING
KOLKATA-700032

Recommendation Certificate

This is to certify that the thesis entitled "Novel ***Bi_2MoO_6/g-C_3N_4 nanocomposite for enhanced photocatalytic degradation of methylene blue dye under visible LED light irradiation****" is prepared and submitted by* ***Snehashis Roy****, be accepted in partial fulfilment of the requirements for the Degree of Master of Civil Engineering with specialization Environmental Engineering from Jadavpur university is absolutely based upon his own work under the super vision of* ***Prof. Ankush Majumdar*** *and that neither his thesis nor any part of this thesis has been submitted for any degree or any other academic award anywhere before.*

Signature of the supervisor and date with office seal

27/06/22

Ankush Majumdar
Assistant Professor
Department of Civil Engineering
Jadavpur University

Professor
Department of Civil Engineering
Jadavpur University
Kolkata-700 032

Countersigned by

27/6/2022

Dean
Faculty of Engineering Technology
Jadavpur University

DEAN
Faculty of Engineering & Technology
JADAVPUR UNIVERSITY
KOLKATA-700 032

27/06/22

Head of Department
Department of Civil Engineering
Jadavpur University

Head
Department of Civil Engineering
Jadavpur University
Kolkata-700 032

3

JADAVPUR UNIVERSITY
DEPARTMENT OF CIVIL ENGINEERING
KOLKATA- 700032

CERTIFICATE OF APPROVAL

This is to certify that this thesis is hereby approved as an original work conducted and presented satisfactory to warrant its acceptance as a prerequisite to the degree for which it has been submitted. It is implied that by this approval the undersigned do not necessarily endorse or approve any statement made, opinion expressed or conclusion drawn therein, but approve the thesis only for the purpose for which it is submitted.

Final Examination for evaluation of thesis

1._____

2._____

3._____

4._____

Acknowledgement

I am extremely thankful and indebted to Prof. Ankush Majumdar, Assistant Professor of Civil Engineering Department, Jadavpur University, for his valuable guidance, constant support and encouragement throughout my thesis work. This thesis would never been completed without his blessings, guidance, constant vigil, careful supervision and inspiration throughout the session.

I am sincerely thankful and obliged to other professors of Environmental Engineering Division Prof. S. Chakraborty, Prof. S.N. Mukherjee, Prof. T. Hazra, Prof. Anupam Deb Sarkar, Prof. A. Dutta, Prof. A. Roy for their constant and thorough guidance during my coursework of Master of Civil Engineering lead me the acquiring of clear concept of Environmental Engineering help me to understand the subject of thesis work as well full completion and submission within stipulated period.

Last but not least, I express my sincere gratitude to all of my batch mates of Environmental Engineering Division for being with me.

Place: Kolkata

Date: 27/06/2022

Snehashis Roy

Snehashis Roy

M.C.E- 2ND Yr.

Class Roll No- 002010402017

Examination Roll No- M4CIV22017

Registration No.-153973 of 2020-2021

Department of Civil Engineering

Jadavpur University

ABSTRACT

Using Bi_2MoO_6 and g-C_3N_4, a novel visible-light-responsive Bi_2MoO_6/g-C_3N_4 nanocomposite photocatalyst was hydrothermally synthesized. The degradation of an emerging dye pollutant, Methylene Blue (MB), under visible LED light irradiation was used to assess the photocatalytic efficiency of the nanocomposite materials. The 10Bi_2MoO_6/g-C_3N_4 nanocomposite was found to have the highest photocatalytic degradation efficiency toward MB at an optimum mass ratio of 10% (Bi_2MoO_6 to g-C_3N_4). Under 60 minutes of visible 20W LED light irradiation, photocatalytic degradation of MB (20 mg/l) by 10Bi_2MoO_6/g-C_3N_4 (1 g/l), was 92.45%, which was about 1.84 and 2.18 times higher as compared to that of pure Bi_2MoO_6 and g-C_3N_4 respectively. This improved performance was linked to the formation of Z-scheme heterojunctions, which resulted in better visible light absorption and less recombination of photo generated electron-hole pairs. Furthermore, the 10Bi_2MoO_6/g-C_3N_4 nanocomposite was found to remove about 92% of COD. The findings not only show how to construct the Bi_2MoO_6/g-C_3N_4 nanocomposite for successful low-cost and energy-efficient photocatalytic degradation of recalcitrant pollutants, but they also encourage the development of similar photocatalysts targeting environmental remediation

CONTENTS

CHAPTER 1: INTRODUCTION……13

CHAPTER 2: LITERATURE SURVEY……17

2.1 Different type of Dyes generated from industry ……..…...17

2.2Harmful effect of dye ……...22

2.3 Available technologies for removal methods of dyes……..23

2.4 Photocatalysis…….....35

CHAPTER 3: MATERIALS AND METHODS …….50

3.1 MATERIALS.....50

3.2 PHOTOCATALYST SYNTHESIS.....50

3.2.1 SYNTHESIS OF Bi_2MoO_6…….50

3.2.2 SYNTHESIS OF g-C_3N_4 NANOSHEETS…….51

3.2.3 SYNTHESIS OF g-C_3N_4/Bi_2MoO_6 NANOCOMPOSITE……..52

3.3 CHARACTERIZATION…….....53

3.4 PHOTOCATALYTIC EXPERIMENT……...53

3.5 RADICAL SCAVENGING EXPERIMENT……...54

3.6 COD DETERMINATION EXPERIMENT…….54

CHAPTER 4: RESULTS AND DISCUSSION.....56

4.1 CHARACTERIZATION OF MATERIALS……..……..56

4.1.1 UV-Vis DRS……..…….50

4.2 PHOTOCATALYTIC ACTIVITY……..58

4.3 RADICAL SCAVENGING EXPERIMENT AND PHOTOCATALYTIC ACTIVITY…….64

4.4 DETERMINATION OF COD REMOVAL EFFICIENCY……67

CHAPTER 5: CONCLUSIONS……...……68

REFERENCES…….……69

LIST OF TABLES

		Page No.
Table 1	Characterization of different classes of dye, mainly used in textile industry and its method of application	20
Table 2	Different types of dye removal processes	31
Table 3	Summary of the recent literature on photocatalytic MB degradation	61

LIST OF FIGURES

		Page No.
Fig 1	Classification of dyes	19
Fig 2	Dye containing effluent from textile industries	20
Fig 3	Pictorial representation of the process taking place in the photocatalytic degradation of dyes on semiconductor surfaces	36
Fig 4	Different types of photocatalyst	38
Fig 5	Schematic diagram for preparation of Bi_2MoO_6	51
Fig 6	Schematic diagram for preparation of g-C_3N_4 nanosheets from Urea	52
Fig 7	Schematic diagram for preparation of Bi_2MoO_6/g-C_3N_4 nanocomposite	53
Fig 8	Closed reflux setup for determination of COD	55
Fig 9	UV-Vis absorbance spectra of Bi_2MoO_6 , g-C_3N_4 and 10Bi_2MoO_6/g-C_3N_4 photocatalyst	57
Fig 10	Tauc plot of Bi_2MoO_6 and g-C_3N_4	57
Fig 11	Photocatalytic degradation efficiency with respect to time using different photocatalysts	59
Fig 12	Pseudo first order reaction kinetics of different nanocomposites towards MB (20 mg/l) degradation	60
Fig 13	Dose variation of 10Bi_2MoO_6/g-C_3N_4(E) nanocomposite for determining the optimum dose towards MB (20 mg/l) degradation	61
Fig 14	Batch experiment for removal of MB using as synthesized photocatalyst under 20W LED light irradiation	62

Fig 15	Initial and final solution of MB under 1 g/l of photocatalyst dose in presence of 20W LED light	62
Fig 16	Photocatalytic degradation efficiency of $10Bi_2MoO_6/g\text{-}C_3N_4$ nano-composites towards MB influenced by radical scavengers	65
Fig 17	Photocatalytic Proposed hetero-junction charge transfer mechanism for the photocatalytic activity over $10Bi_2MoO_6/g\text{-}C_3N_4$ nanocomposite	66
Fig 18	Proposed Z-scheme charge transfer mechanism for the enhanced photocatalytic performance over $10Bi_2MoO_6/g\text{-}C_3N_4$ nanocomposite	66

LIST OF ABBREVEATIONS

AOP	Advance Oxidation Process
BMO	Bismuth molybdenum oxide
BOD	biochemical oxygen demand
BQ	Benzoquinone
CB	Conduction Band
COD	chemical oxygen demand
CR	Congo Red
EDTA	Ethylenediamine tetraacetic acid
IPA	Isopropanol
KHP	Potassium Hydrogen Pthalate
LED	Light Emitting Diode
MB	Methylene Blue
MG	Methyl Green
MO	Methyl Orange
NF	Nano Filtration
RhB	Rhodamine B
RO	Reverse Osmosis
ROS	Reactive Oxygen Species
VB	Valance Band

CHAPTER 1

INTRODUCTION

The dye is the ingredient that turns the water a specific colour. Textile and paper sectors, as well as the medical area, food processing industries, and cosmetics industries, all use it extensively. During the various phases of processing, these industries are the largest users of water and complex chemicals. The procedures release wastewater with high colour, biochemical oxygen demand (BOD), chemical oxygen demand (COD), pH, temperature, turbidity, and hazardous compounds. Around seven lakh tones of various dyes are produced worldwide each year, and during the dyeing process used by various industries, nearly 12% of these dyes are discarded as waste, with about 20% of this waste ending up in the environment, which is a major concern (Wikipedia). Coloured wastewater discharged by industry is not only unsightly, but it also has high biochemical and chemical oxygen demands (BOD_5: 80-6000 mg/L; COD: 150-12000 mg/L) (Al-Kdasi et al., 2004). The direct release of this wastewater into bodies of water such as lakes, rivers, and other bodies of water pollutes the water and harms the flora and fauna. This colourous water is carcinogenic and causes various side effects for human like headache, vomiting, shortness of breath, high blood pressure etc. Methylene Blue (MB) is a dye for wool, linen, and silk fabrics that is widely used in the textile industry (Wahlström et al., 2020). It is also used in pharmaceutical for treatment of Methemoglobinemia. But presence of Methylene Blue (MB) in water causes several health hazards including eye irritation, breathing difficulties, nausea, and diarrhea (Eren et al., 2020). So, in order to achieve desirable water quality, these harmful dyes must be removed from the water in an efficient manner.

Conventional treatment processes like coagulation, flocculation, reverse osmosis etc. are unable to effectively remove the dyes due to their complex structure and produces a huge amount of sludge. As a result, the Advance Oxidation Process (AOP) is used to remove dyes from wastewater efficiently. The combination of ozone (O_3), hydrogen peroxide (H_2O_2) and UV irradiation used in AOP technologies has shown the most promise in treating textile effluent. These oxidants effectively decolourized dyes but did not totally eliminate COD. The goal of any

AOP is to develop and use the hydroxyl free radical ($OH^{\bullet}$) as a powerful oxidant to destroy compounds that are resistant to normal oxidants. Photocatalysis is one of the AOP which can able to degrade the dyesand remove them from the wastewater in a highly efficient manner without producing sludge. When exposed to light irradiation, a semiconductor-based photocatalyst generates electron hole pairs, i.e., electrons exit the valence band and enter the conduction band, producing a pair of electron holes. Photo-generated electron hole pairs will migrate to the semiconductor's surface, where they will undergo a redox reaction(Mohamed et al., 2012). The hole generated in valance bond easily reacts with the H_2O and produces hydroxyls radicals ($OH^{\bullet}$) and the conduction band electron reacts with oxygen to produce superoxide radical anions ($^{\bullet}O_2^-$). These hydroxyls radicals ($OH^{\bullet}$) & superoxide radical anions ($^{\bullet}O_2^-$) are called Reactive Oxygen Species (ROS) which degrades the dyes and converted into CO_2, H_2O & other degradation products (Majumdar & Pal, 2020).

The majority of photocatalytic dye degradation studies have used Titanium dioxide as a photocatalyst, but TiO_2's main disadvantage is that it absorbs only in the UV region due to its 3.2 eV band gap (Viswanathan, 2017). Similarly ZnO is a semiconductor of band gap 3.3 eV which is also widely used for its non toxic nature and wide availability but due to this wide band gap its operational range restricts only UV region (Xiaohua Zhao et al., 2014). TiO_2 and ZnO,in particular, are used as nanorods, nanospheres, thin porous films, nanofibers, and nanowires, or as support for polymeric films(Meng & Juan, 2008). Nanoscale ZnO is a low-cost semiconductor with low toxicity and little impact on the environment. It produces hydroxyl ions more efficiently than TiO2, resulting in visible emissions(Jana & Gregory, 2020). ZnO, on the other hand, has some drawbacks, including a high rate of electron-hole recombination (Anwer et al., 2019). They have a large band gap, fast charge recombination rates, and are only sensitive to UV light (high *hv*), which accounts for about (4–5% of the solar spectrum), they are impractical for large-scale applications. A narrow band gap photocatalyst sensitive to visible light (low *hv*), which accounts for around 52 percent of the solar spectrum, appears to be a more advantageous and long-term solution for dye degradation.

In the presence of visible light, Bismuth-based photocatalysts are among the most effective photocatalysts for degrading organic contaminants. Because of their promising physical and chemical features, such as oxygen ion conductivity, ferroelectricity, and catalytic capabilities,

bismuth-based oxides have sparked a lot of research interest, and they could be used as photochemical catalysts (S. Li et al., 2019; L. Ma et al., 2014; Zhong et al., 2016). Bismuth-containing materials such as $BiVO_4$ (Tokunaga et al., 2001), Bi_2WO_6 (Fu et al., 2006), and Bi_2MoO_6 (Xu Zhao et al., 2007) have a unique layered structure in which perovskite slabs are corner-shared and distorted octahedral are sandwiched between $(Bi_2O_2)^{2+}$ layers. Such a multi layer structure is advantageous for boosting photogenerated carriers' mobility, which is crucial for photocatalysis. As a result, photocatalysts containing bismuth have lately emerged as a common type of visible-light-induced photocatalyst. Among them, bismuth molybdate, γ-Bi_2MoO_6, has demonstrated outstanding photocatalytic activity when exposed to simulated solar light. Bi_2MoO_6open crystal structure and narrow band gap (2.7 eV) make it a promising photocatalytic material (Y. Sun et al., 2013). Various researchers have synthesized Bi_2MoO_6 by different methods like solid state reactions (La Cruz & Lozano, 2010), Co-precipitation (Martínez-de la Cruz & Obregón Alfaro, 2010; Y. N. Zhu et al., 2016), ultrasonic-assistance (Zhou et al., 2007), Molten salt (L. Xie et al., 2008), Hydrothermal (Honghua Li et al., 2008; Phuruangrat et al., 2013; Xu Zhao et al., 2009), Solvothermal (Bi et al., 2007; Chankhanittha et al., 2020; Honghua Li et al., 2008; Tian et al., 2011), Microwave assisted hydrolysis (H. Xie et al., 2007) etc. and reported their efficiencies for removal of different pollutants from wastewater. The predominant active species in the degradation of triazine-containing azo dyes, anionic reactive brilliant red K-2G, reactive brilliant red X-3B, and reactive yellow KD-3G, according to Zhao et al., was $OH^{\bullet}$ (Xu Zhao et al., 2007). Following that, Yin et al. backed up the idea that $OH^{\bullet}$ was the most important species in the photocatalytic process (Yin et al., 2010).

Recently, g-C_3N_4 (Graphitic carbon nitride) has received a lot of attention in photocatalysis due to its small band gap (2.7 eV) which allows it to absorb visible light without modification (He et al., 2014). It is a metal-free polymeric semiconductor as well as its low cost, ease of preparation, great chemical stability, improved electrochemical performance, and environmentally benign nature has all contributed to its popularity (J. Liu et al., 2015; Xiaodong Zhang et al., 2013; B. Zhu et al., 2015). Under visible light, it is employed for organic pollutant degradation, water splitting, CO_2 reduction, and chemical synthesis (Ou et al., 2017; P. Yang et al., 2017; Z. Zhu et al., 2015). However, the poor quantum yield of g-C_3N_4 is due to the quick recombination of photo generated charge carriers, which limits its practical applicability. For that many

researchers has prepared nanocomposites of g-C_3N_4 combining with other material such as WO_3/g-C_3N_4 (Chen et al., 2014),Bi_2O_3/g-C_3N_4 (J. Zhang et al., 2014), $BiVO_4$/g-C_3N_4 (Guo et al., 2014), Fe_3O_4/g-C_3N_4 (Kumar et al., 2013), In_2S_3/g-C_3N_4 (Xing et al., 2014), Bi_3O_4Cl/g-C_3N_4 (Y. Ma et al., 2017) etc which is superior to that of single semiconductors in terms of electron and holes separation and recombination reduction.

In this study, firstly a controlled synthesis of Bismuth Molybdate (Bi_2MoO_6) was done by a facile molten salt aided assembly approached and then a nanocomposites of Bi_2MoO_6/g-C_3N_4 was fabricated by hydrothermal method. Under visible light irradiation, the photocatalysts in the nanocomposites photocatalyzed the degradation of Methylene Blue (MB). The light source for determining the photocatalytic activity of the nanocomposites was a low-intensity, energy-efficient light emitting diode (LED). The photocatalytic efficiency of the Bi_2MoO_6/g-C_3N_4 nanocomposite was found to be significantly higher than that of pure Bi_2MoO_6 and g-C_3N_4. In order to gain insight, the detailed mechanism of photocatalytic degradation of MB by Bi_2MoO_6/g-C_3N_4 nanocomposite was also investigated.

CHAPTER 2

LITERATURE SURVEY

2.1 Different type of Dyes generated from industry

Dyes are the coloured organic compounds, normally used in solution to impart colour to various substances like fabric, paper, leather, hair, drugs, cosmetics, plastics and food material. It's a substance with a suitable colour and the ability to fix itself or be fixed to the fabric. It needs to be quick and resistant to water, dilute acids, alkalis, and a variety of organic solvents. The classification of dyes can be made with the view of three aspects which are (i) source of material (ii) chemical structure of dyes (iii) methods of application.

On the basis of source of material the dyes are classified in two categories which are natural dyes and synthetic dyes. Natural dyes are obtained from natural sources like plants (including fungi and lichens), animals, invertebrates or minerals. Examples of natural dyes are Indigo dyes (from stems and leaves of indigo), Alizarin dyes (from roots of madder plant), Logwoods dyes (from the trunk for black colour to silk and cotton fabrics) etc. These dyes are not that much harmful in nature if present in environment. Synthetic dyes are prepared in labs/factories used for dyeing. The example of synthetic dyes are mordant dyes, azo dyes etc. Majority of dyes used today are synthetic because they are easy to use, cheaper, brighter, fast, have wider range of colours. These synthetic dyes are toxic in nature if present in water source which cause several health hazards for human beings.

A dye molecule has two main components based on its chemical structure: chromophores and auxochromes. Colour is determined by the chromophore, while auxochromes aid in fibre attachment. On the basis of chromophores & auxochrome the dyes are nitro & nitroso dye, azo dye, triarylmethane dye, anthraquinone dye, Indigo dyes etc. In nitro and nitroso dye contain nitro group ($-NO_2$) and nitroso group (-NO) as the chromophores respectively and hydroxyl group (-OH) as auxochrome. One of the examples of nitro dye is Naphthol yellow S and nitroso dye is Gambine-Y. In azo dyes Azo group (-N=N-) is present as primary chromophore in their molecular structure which is present between two aromatic rings. Tartrazine (yellow), Methyl

Orange, Congo Red, Bismarck Brown, Chrysoidine, and other azo dyes are examples. Azo dyes account for 60-70% of dyes used in food and textile production. A central carbon is bonded to three aromatic rings in triarylmethane dyes, one of which is quinoid. The examples of triarymethane dyes are Malachite Green (used as a direct dye for wool and silk), Crystal violet, and Phenolphthalein etc. In Anthraquinone dye Anthraquinone ring is the chromophore and -OH, $-SO_3H$, $-NH_2$ as auxochrome. One of the examples of this dye is Alizarin-red textile dye. In Indigo dyes have carbonyl chromospheres and indigoid structure (-CO=C=C-CO-). These dyes are used in cotton yarn, which is primarily used to make blue jeans denim cloth.

On the basis of methods of application the dyes are classified as Acidic dyes, Direct dyes, Vat dyes, Mordant dyes, Azoic dyes, Disperse dye, Sulphur dye, Basic dyes or cationic dyes, Reactive dye etc. Acid dyes are sodium salts of sulphonic and carboxylic acids. Acid dyes are anionic dyes that are water soluble. Nylon, wool, silk, and modified acrylics are all treated with it. Paper, leather, inkjet printing, food, and cosmetics all use them. Methyl Orange (MO) is an example of an acid dye. A neutral or slightly alkaline dye solution can be used to apply direct dye. Auxochromes that are acidic or basic are present. It has a polar nature and a strong affinity for cellulosic fibre. Martius yellow is an example of a direct dye. Insoluble in water, vat dyes are reduced in an alkaline bath and applied to cellulosic fibres as soluble leuco salts. In the fiber, the leuco forms are re-oxidized to the insoluble keto forms. Examples of vat dyes are anthraquinone and indigoid etc. Mordant dyes are used with the help of salts. Mordants – Al or Cr oxides salts (Sodium or Potassium dichromate mordant is added in the dye bath) are most suitable for wool and nylon. One of the examples of Mordant dyes is Alizarin. In azoic dyes two soluble components usually phenol or napthol or aniline are impregnated in the fiber to form an insoluble colour molecule. The examples of these type of dyes are Aniline phenyl azo, Para Red etc. Disperse dyes are insoluble in water and it is applied to hydrophobic fibers from an aqueous dispersion. It can form a colloidal dispersion in water. Crystal structure of fabric absorbs the colloidal particles. These dyes are used for synthetic fibers viz. polyester, nylon, cellulose acetate and acrylic fibres. The example of disperse dye is Duranol Red 2B. Sulphur dyes are used primarily for cotton and rayon, offers good wet fastness and variety of colours. It is not applicable for wool or silk. The example of sulphur dye is Indigo vat blue. Basic dyes, also known as cationic dyes, are water-soluble and appear in solution as coloured cations. Applied to

paper, polyacrylonitrile, modified nylons and modified polyester. The examples of these dyes are Chrysoidine, Methylene Blue. In reactive dye chromophore group that reacts with the substrate, forms a covalent bond with the fiber usually cotton, wool and nylon. Examples of reactive dyes are Azophthalocyanine, formazan and anthraquinone etc.

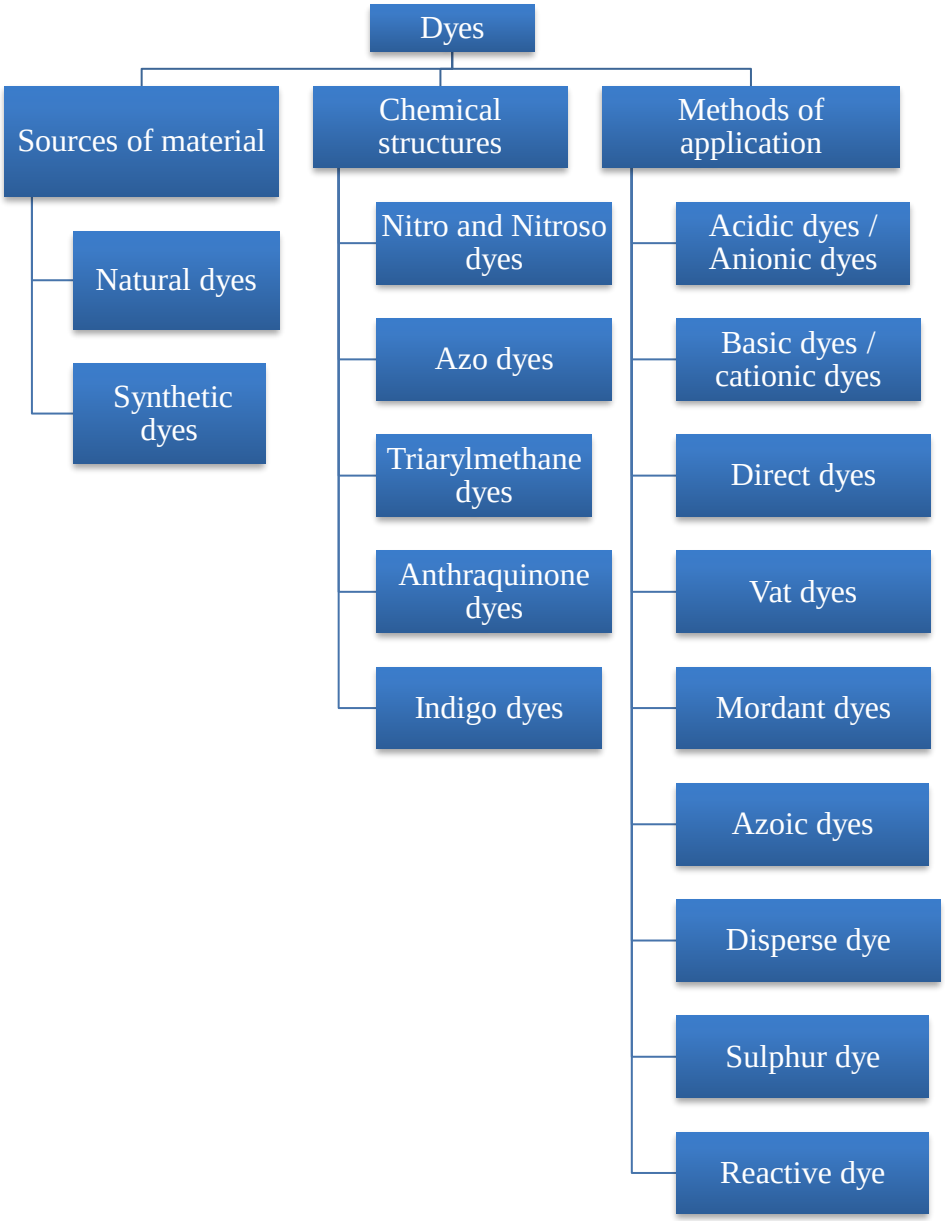

Fig 1: Classification of dyes

Dyes are mainly used in textile industries so textile industry effluent contains various types of colour. Apart from that paint producing industry, paper industry, food processing industry also uses dyeto impart colour. So this industry also emits colourous wastewater.

Fig 2: Dye containing effluent from textile industries

Different types of dyes used in textile industry and there method of applications are tabulated in below

Table 1: Characterization of different classes of dye, mainly used in textile industry and its method of application (Akbari et al., 2002; Easton, 1995; Lau and Ismail, ; 2009 Hees et al., 2002).

Class	Characteristics	Substrate (fibre)	Dye-fibre interaction	Method of application
Acid	Water soluble, anionic	Silk, Nylon, wool	Electrostatic, Hydrogen bonding	Applied from neutral to acidic dye baths
Basic	Water soluble, Cationic	Modified nylon, polyester	Electrostatic attraction	Applied from acidic dye baths
Direct	Water soluble,	leather, nylon, Cotton,	Intermolecular	Applied from neutral

	Anionic	rayon	forces	or slightly alkaline baths containing additional electrolytes
Disperse	Very low water solubility	Polyester, poly-amid , acrylic acetate, plastic	Hydrophobic-Solid state mechanism	Fine aqueous dispersions often applied by high temperature pressure or lower temperature carrier methods
Reactive	Water soluble, anionic	Cotton, wool, nylon, silk	Covalent bonding	Reactive site on dye reacts with functional group on fibre to bind dye covalently under influence of heat and pH(alkaline)
Sulfur	Insoluble, colloidal	Cotton, rayon	Covalent bonding	Aromatic substrate vatted with sodium sulfide and reoxidized to insoluble sulfur-containing products on fibre
Vat	Insoluble, colloidal	Cotton, rayon	Impregnation and oxidation	Water insoluble dyes solubilised by reducing with sodium hydrosulfite, then

	exhausted on fibre and re-oxidised

2.2 Harmful effect of dye

The above-mentioned classification of dyes, of which synthetic dyes are the most important, is our primary concern. Because synthetic dyes are widely used in products such as clothing, leather accessories, paints, papers, furniture, and plastics nowadays. The industry uses many different types of colouring dyes, including Methylene Blue (MB), Methyl Orange (MO), Methyl Green (MG), Rhodamine B (RhB), Congo Red (CR), and others. Methylene Blue (MB) is a dye for wool, linen, and silk fabrics that is widely used in the textile industry (Wahlström et al., 2020). Methyl green is a cationic dye used in the medical profession, as well as the paper, textile, leather, food, and cosmetic industries, to dye cotton, silk, wool, and nylon, as well as waxes, plastics, oils, fats and varnish (Eren et al., 2020). Around seven lakh tones of various dyes are produced worldwide each year, and during the dyeing process used by various industries, nearly 12% of these dyes are discarded as waste, with about 20% of this waste ending up in the environment, which is a major concern (Wikipedia). Coloured wastewater discharged by industry is not only unsightly, but it also has high biochemical and chemical oxygen demands (BOD5: 80-6000 mg/L; COD: 150-12000 mg/L) (Al-Kdasi et al., 2004). Expulsion of unwanted sewage into the environment, which causes pollution of nearby soil and water, is a major environmental threat in textile industrial dye markets (Potti & Srivastava, 2013). Even a low concentration of organic dye, such as 1-3 mg/L, is extremely toxic to humans (Benedek et al., 2018). The dyes cause dermatitis, severe eye irritation, breathing problems, and infection of the nasal septum, among other health problems (Lou & Zeng, 2003). Because dyes are water-soluble organic chemicals, they hinder the passage of light through water, lowering photosynthesis rates and lowering water oxygen levels, harming the entire aquatic biota (Imran et al., 2015). To various microorganisms and fish species, dyes are also carcinogenic and mutagenic. Methylene Blue (MB) has a number of negative health effects, including eye irritation, breathing difficulties, nausea, and diarrhea (Eren et al., 2020). Methyl Green (MG) is a hazardous water pollutant because it causes chemical burns in the gastrointestinal tract and oral cavity, which can

lead to perforation of the stomach and oesophagus; its entry into the bloodstream through abrasions, cuts, or lesions can cause systemic damage with serious health consequences; and it can harm the respiratory tract, increasing the risk of chronic bronchitis and pneumonia. If not properly handled, these synthetic harmful dyes can remain in the environment for a long time (Chaudhary et al., 2020). As a result, in order to achieve long-term water quality, these dyes must be removed from the water in an efficient manner.

2.3 Available technologies for removal methods of dyes

The majorities of synthetic dyes are poisonous in nature and constitute a risk to aquatic life. To meet with tight environmental requirements, numerous traditional methods for removing colours from water and wastewater have been used, including chemical coagulation, electro coagulation, adsorption, membrane processes, biological processes, and so on. These methods are described as follows

(i) Chemical coagulation & flocculation:

Coagulation and flocculation are commonly employed as physicochemical procedures for cleaning industrial wastewater because they destabilize and create flocs, which remove colloidal particles, very small solid suspensions, and a few soluble chemicals that were previously present in the wastewater. According to several researches, the coagulation process has proven to be the most effective approach when compared to other processes such as anaerobic reduction, oxidation, and adsorption, and it is also one of the simplest and cheapest procedures that may be easily employed in industrial settings (Kos, 2016). Coagulation removes around 70 to 80 percent of the colour and reduces the concentration of organic chemicals by about the same amount. The efficacy of this procedure is determined by the qualities of raw wastewater, as well as the temperature and pH of the solution, as well as the type and dosage of coagulants used, and the mixing time (Mokif, 2019). Inorganic salts like alum or ferric chloride, as well as synthetic organic polymers, are common coagulants. Although chemical coagulants are used to remove colours and suspended particles from wastewater, they have a number of drawbacks, including their impact on humans by creating diseases like Alzheimer's disease, which is caused by inorganic salts, and some of them are also carcinogenic in nature.

Chemical coagulation is a complex process involving a number of interconnected characteristics, thus it's crucial to know how well a coagulant will perform under specific conditions. As a cogulation, alum, ferric chloride, ferric sulphate, and magnesium chloride can be employed. Destabilization is affected differently by different coagulants. The higher the counter ion's valence, the more destabilizing it is and the lower the required coagulation dose. Positively charged polymers will prevail when the pH is below the isoelectric point of metal hydroxide and colloids are precipitated by various coagulants supported by a suitable polymer. Adsorption of these positively charged polymers can destabilize negatively charged colloids by charge neutralization. Anionic polymers will predominate above the isoelectric point, when particle instability may occur due to adsorption and bridge formation. When a large dose of metal ions (coagulant) is used, a sufficient degree of oversaturation occurs, resulting in the rapid precipitation of a large amount of metal hydroxide, enmeshing the colloidal particles known as sweep flocs (Peavy et al., 1985). Monomeric and polymeric ferric species are produced when Fe (III) salts are used as coagulants, with the generation of monomeric and polymeric ferric species being pH dependent. According to several studies, the natural colour of ferric chloride solution is acidic, but successful removal can only be done when the pH is close to neutral, therefore adding a base to keep the pH stable becomes a must. Lime or sodium hydroxide (NaOH) might be used for this. Lime, on the other hand, may result in more sludge. The use of polyelectrolyte as a coagulant aid, on the other hand, often improves the coagulant's performance. As can be observed, the ideal pH for alum is close to neutral, allowing for greater colour removal efficiency. Furthermore, the inclusion of polyelectrolyte improves the colour removal performance in general. The vast amount of sludge generated by this technique, however, makes it unappealing. Magnesium chloride's optimal pH ranges from 9 to 12. When used with lime, it provides excellent colour removal. However, it produces a huge amount of sludge, which may provide a sludge disposal concern as well as additional costs. Because of the enormous volume of sludge generated and the formation of basic effluent after treatment, alum and magnesium chloride may not be regarded good coagulants. Though both ferric chloride and alum have a high efficiency, ferric chloride has lower colour removal effectiveness at low concentrations. However, when ferric chloride is combined with a little amount of cationic polymer, a considerable improvement in colour removal has been recorded.

(ii) Electro coagulation:

The electro coagulation process is a type of colour removal from wastewater electrochemical technology. The unique properties of environmental compatibility, safety, and versatility drew a lot of attention to this technology. To meet the needs of many sectors, electrochemical technology competes with other traditional technologies such as precipitation, evaporation, ion exchange, and solvent extraction. Electrochemical technologies are superior to physicochemical and membrane technologies in general, especially when it comes to removing colour from wastewater, because they use the electron as a single reagent and do not produce solid residues. Coagulation, adsorption, precipitation, and flotation are the main methods of pollutant removal during electro coagulation. Electro coagulation provides several advantages over biological treatments, including a smaller footprint due to a shorter reaction time, lower sludge production compared to chemical coagulation, lower equipment and operation costs, and ease of use.

Coagulants are generated in situ during electro coagulation by electro oxidation of sacrificed anodes. The suspended particles or precipitates are then destabilized and aggregated by aluminum or iron hydroxide flocs, which adsorb dissolved contaminants. Because aluminum and iron are inexpensive and readily available, they are the most commonly used materials in electro coagulation. The effectiveness of electro coagulation with aluminum electrodes to remove Reactive Red198 (RR198) from aqueous solution was investigated by Dalvand et al. Variables such as voltage variation, reaction time, inter electrode distance, initial dye concentration, electrolyte concentration, and electrode connection mode were studied to see how they affected dye removal percentage. They also looked into the best operating conditions in terms of electrical energy consumption and electrode consumption. The structure of Reactive Red198 (RR198) is made up of different groups. At 288, 373, and 518 nm, these groups have three different absorbance peaks. The benzene, naphthalene, and azo-linkage peaks could all be attributed to benzene, naphthalene rings, and azo-linkage, respectively. Depending on the type of electrode material used, dye removal during electrochemical processes could be due to dye molecules being broken down into smaller organic compounds. To assess the dye removal mechanism by electro coagulation, the absorbance of raw and treated wastewater was measured at three absorption wavelengths of 288, 373, and 518 nm. In addition, absorbance at 254 nm was measured to determine the presence of aromatic compounds in the solution caused by dye

cleavage. During the electro coagulation treatment, all of the absorbance peaks decreased and were almost completely gone after about 30 minutes. The decrease in absorbance peaks indicated that dye molecule adsorption on flocs was the primary mechanism for dye removal. The removal of RR198 did not result in azo-linkage cleavage or the production of other by-products. The high COD removal rate (84.1%) confirms that the cleavage azo group plays only a minor role in dye removal. Low decomposition of dye molecules to small organic substances via electro-oxidation may explain the lower COD removal compared to dye removal.

(iii) Membrane process (Reverse Osmosis (RO) & Nano Filtration (NF)):

Membranes are widely used in a variety of separation processes because of their ability to control materials passing through the membrane, resulting in a high degree of separation that is always achieved, making these processes widely acceptable. The membrane is a barrier that allows some substances to pass through it (permeate) while preventing others from doing so (retentate) in a very specific way. Membranes can be used to separate fluids, dissolved solids, suspended solids, and colloidal dissolved solids. The ability to remove or recover valuable or harmful components, as well as the ability to close water systems, which reduces the consumption of fresh water, are the main characteristics of membrane processes in the treatment of consumables. The use of membrane processes allows wastewater to be purified to a level that is difficult to achieve with traditional methods. Reverse Osmosis (RO) and Nano Filtration are the most widely used and significant membrane filtration techniques (NF). The operating pressure of NF is between 5 and 40 bars, and the membrane pore size is between 0.5 and 2 nm. On the one hand, it's used to separate sugars, other organic molecules, and multivalent salts from monovalent salts, ions, and water, and on the other hand, it's used to separate monovalent salts, ions, and water. In RO or hyper filtration, the membrane pore size is in the range of 0.5 nm. Operating pressures in RO are usually between 7 and 100 bars. The importance of membrane processes is demonstrated by the membrane areas installed in various industrial sectors. RO membranes are a popular choice for treating contaminated drinking water supplies because of their ability to remove both organic and inorganic compounds. Hardness, colour, a variety of bacteria and viruses, as well as organic contaminants like agricultural chemicals and tri-halo-methane precursors, can all be removed simultaneously using reverse osmosis. Avlonitis et al.

looked at effluents from the cotton textile industry that were treated with a nanofiltration membrane to reduce the amount of water that was discarded while also allowing the treated water to be reused (Avlonitis et al., 2008). The results showed that NF membranes were capable of completely decolourizing the cotton dye effluent and reducing the total salt concentration by more than 72%. Even at high recoveries and low pressures, these membranes can produce high-quality water that can be reused. Gozálvez-Zafrilla et al. looked into the treatment of secondary effluent for wastewater reuse in the textile industry (Gozálvez-Zafrilla et al., 2008). They used (NF90) membrane in their research. The results showed that NF90 had the highest salt rejection and a 99 percent COD reduction (75-95%). The levels of COD removal and salt rejection were unaffected by fouling, and the permeate quality allowed for a high flux percentage to be recovered after cleaning. Abid et al. used the RO & NF process to test acid red, reactive black, and reactive blue dye (Abid et al., 2012). They discovered that RO and NF membranes can effectively remove dye from wastewater, and that dye removal was proportional to applied pressure, pH, TDS, and dye concentration in the feed solution, but not to feed temperature.

(iv) Biological process:

The biological process employs microorganisms such as fungi, bacteria, and algae, which are capable of biodegrading and absorbing dyes found in wastewater. The use of microorganisms to remove dyes from wastewater has a number of advantages, including a low cost, an environmentally friendly process that produces less secondary sludge, and nontoxic final products for complete mineralization. Many studies have been conducted that show the ability of microorganisms like Cunninghamellaelegans, Aspergillusniger, Bacillus cereus, Chlorella Spand, and Citrobactersp to remove dye from industrial wastewater. The most important factors influencing the decolourization effectiveness of microbial activity are the adaptability and activity of each microorganism. Colour is removed using biological treatment, but because most dyes are designed to resist light and oxidation degradation, they are less likely to be treated with traditional aerobic therapy. The removal of water-soluble dyes by aerobic processes is a particular problem. On wastewater sludge, some of these dyes are adsorbed. Direct biological treatment with bacteria or fungi is also possible, but the nutritional and physiological requirements of microorganisms limit the applicability of these bioremediation methods. The use

of enzymes to replace traditional non-biological methods has gained popularity as a result of research into effective and environmentally friendly oxidation techniques. Biological treatment methods have proven to be effective in reducing dye house effluents, and when used properly, they are less expensive to operate than other methods. In the water treatment process which combine chemical and biological, or physical and biological, have also been found to be effective. Biological treatment of textile azo dyes has been shown to be an effective method for degrading all dye materials while also overcoming many of the disadvantages of physicochemical processes. Both aerobic and anaerobic metabolism can be used by microbes and their enzymes to degrade dye. Several studies have been published on the degradation of environmental contaminants by different bacteria. Many bacteria have been identified as relying solely on hydrocarbons. Bacteria with hydrocarbon-degrading bacteria have the ability to degrade hydrocarbons. Because they are biodegradable and easy to maintain, these bacterial bio flocculants provide an affordable and clean alternative for replacing or supplementing current treatment processes to remove dyes from wastewater effluents. Daneshvar et al. looked into the ability of microalgae Cosmarium species to decolourize a solution containing Malachite Green, a cationic textile dye (Daneshvar et al., 2007). They looked at algal stability and reusability during repeated decolourization operations, as well as the relationship between kinetic properties and dye concentration and other rate-dependent environmental variables (temperature, pH, dye concentration, and algal concentration).

(v) Adsorption with conventional adsorbent (activated carbon):

Adsorption is the method of choice and produces the best results among the many dye removal techniques available because it can be used to remove a variety of colouring materials (Jain et al., 2003; Ho and McKay, 2003; Derbyshire et al., 2001). If the adsorption system is properly designed, the treated effluent will be of high quality. Depending on the nature of the forces involved, adsorption processes can be classified as either physical or chemical. Adsorbate/adsorbent interaction, adsorbent surface area and pore structure, surface chemistry, nature of the adsorbate, effect of other ions, particle size, pH, temperature, contact time, and other physico-chemical factors all influence the adsorption process. In comparison to other techniques such as coagulation, flocculation, precipitation, and activated sludge, the adsorption technique has proven to be more effective and convenient due to its low cost, simple design, easy

handling, and sludge-free cleaning operations. Adsorption processes are a viable treatment option, particularly when the adsorbent is cheap and readily available. Activated carbon is the most widely used adsorbent among commercial adsorbents. The use of activated carbon as a dye removal technique has been highlighted as a viable option. Activated carbon has an extremely high affinity for many types of dyes, including basic dyes, due to its unique molecular structure. Because of its excellent adsorption ability, activated carbon is currently used as a sorbent in most commercial systems to remove dyes from wastewater. One of the best available control technologies, according to the US Environmental Protection Agency, is activated carbon adsorption (Derbyshire et al., 2001). Activated carbon, on the other hand, is a preferred sorbent, but its widespread use is limited due to its high cost. Efforts have been made to find low-cost alternative adsorbents in order to reduce treatment costs. El Qada et al. investigated activated carbon and compared the adsorption capacity of three different activated carbons (PAC1 and PAC2 developed at QUB for this work, and commercially available Filtrasorb 400) (El Qada et al., 2008). Basic dyes were chosen as the model adsorbates because: I they are toxic; (ii) their tinctorial value is very high, with less than 1 ppm of dye visible in solution; and (iii) basic dyes ionize in solution, forming cations with a high affinity for negatively charged adsorbent surfaces, facilitating adsorption processes.

(vi) Adsorption with non-conventional adsorbents (fly ash):

Aside from traditional adsorbents like activated carbon, a variety of approaches to developing cheaper and more effective adsorbents have been investigated. Several researchers have proposed a variety of non-traditional low-cost adsorbents, including natural materials, biosorbents, and waste materials from industry and agriculture. These materials could be used to remove dyes from solutions as sorbents. Biosorbents (chitosan, peat, biomass), clay materials (bentonite, kaolinite), zeolites, siliceous materials (silica beads, alunite, perlite), agricultural wastes (bagasse pith, maize cob, rice husk, coconut shell), industrial waste products (waste carbon slurries, metal hydroxide sludge), and others have all been reported as sorbents (starch, cyclodextrin, cotton). G. Crini looked at the technical feasibility of using nontraditional low-cost adsorbents to remove dye from contaminated wastewater (Crini, 2006). He believes that low-cost adsorbents have a lot of potential for commercial applications in the future. Chitosan-based

sorbents, in particular, have demonstrated superior dye removal capabilities when compared to activated carbon. Despite a number of papers on low-cost adsorbents being published, there is still a scarcity of information containing a comprehensive comparison of sorbents. Although much progress has been made in the field of low-cost sorbents, much more work is needed to I predict the performance of adsorption processes for dye removal from real industrial effluents under a variety of operating conditions, (ii) better understand adsorption mechanisms, and (iii) demonstrate the use of low-cost sorbents on an industrial scale. For the removal of crystal violet and rosaniline hydrochloride (basic fuchsine) from wastewater, Mohan et al. used fly ash generated in thermal power plants as a low-cost adsorbent(Mohan et al., 2002). They discovered that as the temperature rises, the adsorption of the two dyes increases, indicating that the process is endothermic. Both the Freundlich and Langmuir models can be used to fit the data and estimate model parameters, according to the findings. Overall, the nonlinear Freundlich adsorption isotherm fits the data better. Crystal violet and basic fuchsine dyes have higher or comparable adsorption capacities on fly ash than other adsorbents used for the same or other cationic dyes. According to their findings, fly ash can be used as an effective adsorbent for dye removal.

(vii) Advanced oxidation process (AOP):

Traditional oxidation treatments have struggled to oxidize dyestuffs and organic compounds with complex structures at low concentrations or when they are particularly resistant to oxidants. Advanced oxidation processes (AOPS) have been developed to generate hydroxyl free radicals using various techniques to alleviate the problems mentioned. The AOPS processes, which combine ozone (O_3), hydrogen peroxide (H_2O_2) and UV irradiation, to treat textile wastewater, have shown the most promise. These oxidants effectively decolourized dyes but did not completely eliminate COD. Any AOP's goal is to generate and use hydroxyl free radical ($OH^{\bullet}$) as a strong oxidant to destroy compounds that cannot be oxidized by conventional oxidants. Advanced oxidation processes are defined by the production of $OH^{\bullet}$ radicals and attack selectivity, which is a useful property for an oxidant. The fact that AOP can be used in a variety of ways for $OH^{\bullet}$ adds to their versatility. Combining O_3, H_2O_2, TiO_2, UV radiation, electron-

beam irradiation and ultrasound is a common way to speed up the production of $OH^{\bullet}$. The most promising are O_3/H_2O_2, O_3/UV and H_2O_2/UV for oxidizing textile wastewater.

The various types of dyes removal processes, significant factors, removal efficiency, advantages and disadvantages are compiled in below table.

Table 2: Different types of dye removal processes

Technology	Target Dye	Significant factors	Results	Advantages / Disadvantages	References
Chemical Coagulation	Reactive dye, sulfur dye, acid dye, disperse dye,	(i) Optimum dose of coagulant: alum, magnesium chloride, ferric chloride, ferrous sulfate (ii) Coagulant aids: Poly-acrylamide based polymer is used with alum &Polyelectrolyte Can be used for ferric chloride, magnesium chloride & ferrous sulfate (iii) pH of the solution: alum-(5.3-7), ferrous sulfate-(9.4-12.5), ferric chloride-(6-8.3), magnesium	Reactive dye: 98% (alum), 71% (ferric chloride), 90% (ferrous sulfate), 85% (magnesium chloride) Disperse dye: 78.9% (alum), 71% (ferric chloride), 98% (magnesium chloride) Sulfur dye: 100% (ferric chloride), 90% (ferrous sulfate) Acid dye: 98% (alum)	**Advantages:** It is an economically feasible process and efficiently removes the colour from wastewater **Disadvantages:** Huge sludge production is the major disadvantage of this process	(Tan et al., 2000) (Georgiou et al., 2003) (Golob et al., 2005) (Bidhendi et al., 2007) (Gao et al., 2007) (El-Gohary and Tawfik, 2009)

		chloride-(11-12)			
Electro-coagulation	reactive red 198	voltage, electrode connection mode, electrical energy consumption, inter electrode distance, dye concentration and electrolyte concentration;	i) Dye removal follows first order kinetics; ii) 98.6% dye removal and 84% COD removal;	**Advantages:** requires smaller space, easy operation, ecofriendly process, cost effective method; **Disadvantages:** sludge Generation	(Kobya et al., 2007) (Dalvand et al., 2011) (Latha et al., 2017)
Membrane processes: reverse osmosis (RO), nano-filtration (NF)	acid red, reactive blue, reactive black,	RO: membrane pore size (0.5 nm), operating pressure (7–100 bars); NF: membrane pore size (0.5–2 nm),operating pressure (5–40 bars);	i) NF method consumes half of the electrical power compared to RO; ii) NaCl in dye solution increases dye removal efficiency; iii) pH, TDS, applied pressure and dye concentration show good effect on dye removal; iv) Feed temperature shows bad effect on dye removal;	**Advantages:** higher removal potential with lower effective cost; **Disadvantages:** production of concentrated sludge;	(Avlonitis et al., 2008) (Gozálvez-Zafrilla et al., 2008) (Abid et al., 2012)

Biological processes: Green algae (Cosmarium species)	Malachite green	Dye concentration, Algal concentration, solution pH, and temperature;	i) Dye decolourization rate is described with Michaelis-Menten model; ii) Optimum pH is 9; temperature (5–45 C) has positive effect on decolourization rate; iii) Optimal kinetic parameters: v_{max} (maximum specific decolourization rate) is 7.63 mg dye g $cell^{-1}h^{-1}$ and K_m (dissociation constant) is 164.57 ppm;	**Advantages:** Algae are available in worldwide in different kinds of habitats, good capability for verity of dye decolourization, economically feasible, publicly acceptable process; **Disadvantages:** slow process, needs to be performed under optimal favorable conditions;	(Crini, 2006) (Daneshvar et al., 2007)
Activated carbon (AC) adsorption	Methylene blue, basic yellow 21, basic red 22	AC surface area, surface chemistry, pore structure; adsorbent dose, and solution pH;	i) Three adsorption isotherm models (Langmuir, Freundlich and Redlich-Peterson) have been used, Redlich-Peterson	**Advantages:** very effective adsorbent, high adsorption capacity; **Disadvantages:**	(Crini, 2006) (El Qada et al., 2008)

			model gave best fit; ii) Alkaline pH and low pore size of AC favored dye adsorption;	non-destructive process, AC regeneration is very costly;	
Adsorption with non-conventional adsorbents: Fly ash from thermal power plant	Basic violet, Basic fuchsine	Adsorbent particle size, adsorbent dose, solution pH, and temperature;	i) Langmuir and Freundlich adsorption isotherm have been used, nonlinear Freundlich model gave better fit; ii) Negative free energy value and positive enthalpy value suggest spontaneous and endothermic process; iii) Dye adsorption follow 1storder kinetics;	**Advantages:** cost effective adsorbent, high adsorption capacity; **Disadvantages:** non -destructive process, expensive regeneration process;	(Crini, 2006) (Mohan et al., 2002)
Advanced oxidation processes (AOPs)	Several textile dyes	Ozone (O_3), hydrogen peroxide (H_2O_2), wavelength of ultraviolet (UV) light, O_3/UV, H_2O_2/UV, O_3/H_2O_2/UV, solution pH, dye	i) In O_3/UV process hydroxyl radical ($OH^{\bullet}$) is produced after activation of O_3 by UV(λ = 254 nm); ii) H_2O_2/UV also produces $OH^{\bullet}$ radical for dye degradation;	**Advantages:** complete mineralization achieved in presence of $OH^{\bullet}$; no sludge generation, appropriate	(Al-Kdasi et al., 2004)

	concentration, and temperature;	iii)Among all AOPs $O_3/H_2O_2/UV$ shows highest efficiency for dye degradation;	process for recalcitrant dyes; **Disadvantages:** several by-product formations, less economic feasibility;

2.4 Photocatalysis

Photocatalysis for water decontamination was first recognized in the 1980s, when photocatalytic mineralization for various halogenated hydrocarbons was successfully conducted (Pruden & Ollis, 1983). Photocatalysis is an Advance Oxidation Process (AOP) where, when exposed to light irradiation, a semiconductor-based photocatalyst generates electron hole pairs, i.e., electrons exit the valence band and enter the conduction band, forming a pair of electron holes. Photo-generated electron hole pairs will move to the semiconductor's surface, where they will undergo a redox reaction (Mohamed et al., 2012). The hole generated in valance bond easily reacts with the H_2O and produces hydroxyls radicals ($OH^{\bullet}$) and the conduction band electron reacts with oxygen to produce superoxide radical anions ($^{\bullet}O_2^-$). The mechanism for generation of hydroxyl radicals and superoxide radical anions are shown in following equations.

$$\text{Photocatalyst} + h\upsilon \rightarrow e^-_{cb} + h^+_{vb} \quad (1)$$

$$H_2O + h^+_{vb} \rightarrow OH^{\bullet} + H^+ \quad (2)$$

$$OH^- + h^+_{vb} \rightarrow OH^{\bullet} \quad (3)$$

$$OH^{\bullet} + OH^{\bullet} \rightarrow H_2O_2 \quad (4)$$

$$H_2O_2 + h\upsilon \rightarrow 2\ OH^{\bullet} \quad (5)$$

$O_2 + e^-_{cb} \rightarrow {}^{\bullet}O_2^-$ (6)

${}^{\bullet}O_2^- + H_2O_2 \rightarrow OH^{\bullet} + O_2 + OH^-$ (7)

$H_2O_2 + e^-_{cb} \rightarrow OH^{\bullet} + OH^-$ (8)

These hydroxyls radicals ($OH^{\bullet}$) & superoxide radical anions (${}^{\bullet}O_2^-$) are called Reactive Oxygen Species (ROS) which degrades the dyes and converted into CO_2, H_2O & other degradation products. The pictorial representations of dye degradation are shown in below.

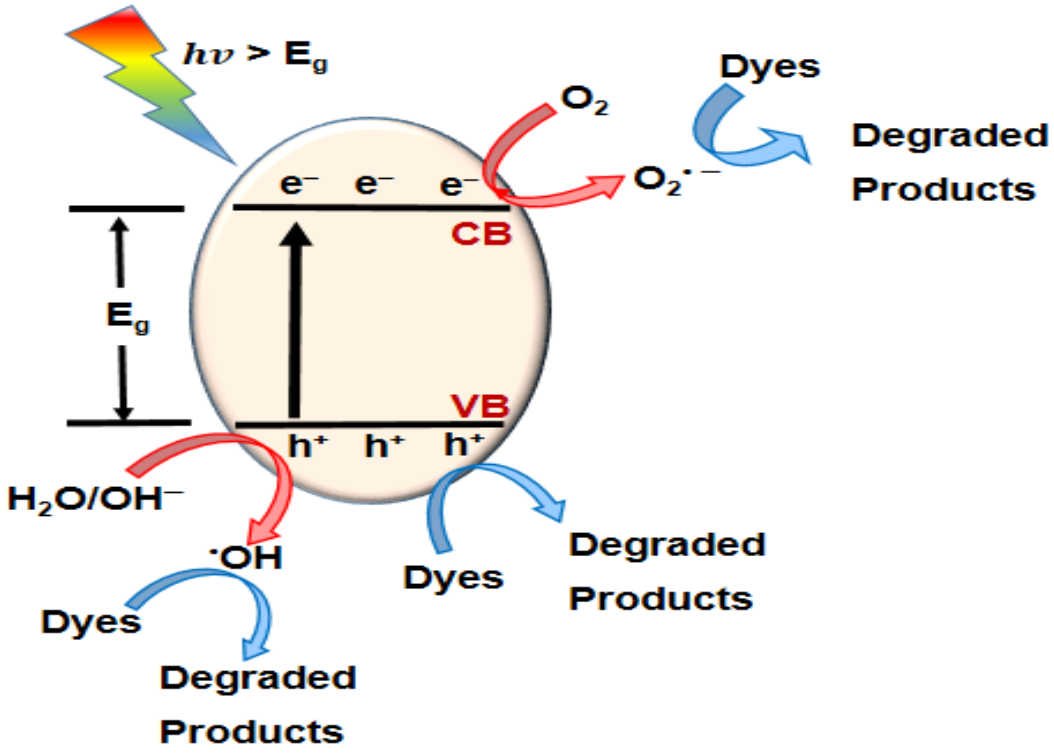

Fig 3: Pictorial representation of the process taking place in the photocatalytic degradation of dyes on semiconductor surfaces

The photocatalyst's efficacy in degrading dye is primarily determined by three key factors: (1) band-gap energy (Eg): Photocatalysts with a wide band-gap are sensitive to UV light, while photocatalysts with a narrow band-gap are sensitive to visible light; (2) band edge potentials, i.e., the potentials of VB and CB: ROS can only be generated when the CB potential is less than the reduction potential of O_2 to ${}^{\bullet}O_2^-$ (− 0.33 eV vs. NHE) and/or VB potential is more positive than

standard oxidation potential of $OH^{\bullet}/H_2O$ (+ 2.68 eV vs. NHE) or $OH^{\bullet}/OH^{-}$ (+ 1.99 eV vs. NHE) (Panneri et al., 2017). If this is not the case, the h^+ in the VB reacts directly with the pollutant. The more ROS produced, the higher the semiconductor's efficiency; and (3) rate of e^{-}– h^+ pair recombination: Recombination of e^{-}– h^+ pairs reduces catalyst efficiency due to the strong Columbic attraction between them. Recombination causes the e to revert to the VB without undergoing the reduction reaction, resulting in the formation of $^{\bullet}O_2^-$ (Pelaez et al., 2012). As a result, these three important factors should be considered when selecting a photocatalyst.

Different types of photocatalyst:

The majority of photocatalytic dye degradation studies have used Titanium dioxide as a photocatalyst, but TiO_2'smain disadvantage is that it absorbs only in the UV region due to its 3.2 eV band gap (Viswanathan, 2017). Similarly ZnO is a semiconductor of band gap 3.3 eV which is also widely used for its non toxic nature and wide availability but due to this wide band gap its operational range restricts only UV region (Xiaohua Zhao et al., 2014). The semiconductors especially TiO_2 and ZnO are employed as nanorods, nanospheres, thin porous films, nanofibers and nanowires or supported on polymeric films (Meng & Juan, 2008). Nano scale ZnO is a low-cost semiconductor with low toxicity and little impact on the environment. It produces hydroxyl ions more efficiently than TiO2, resulting in visible emissions(Jana & Gregory, 2020). ZnO, on the other hand, has some drawbacks, including a high rate of electron-hole recombination(Anwer et al., 2019). However, because TiO_2 and ZnO have a wide band gap, fast charge recombination rates, and are only sensitive to UV light (high hv), which accounts for only 4–5% of the solar spectrum, they are impractical for large-scale applications. From this perspective, a narrow band gap photocatalyst sensitive to visible light (low hv), which accounts for about 52 percent of the solar spectrum, appears to be a more favorable and long-term solution for dye degradation. The various types of photocatalysts are depicted in the flow diagram below and are described as follows:

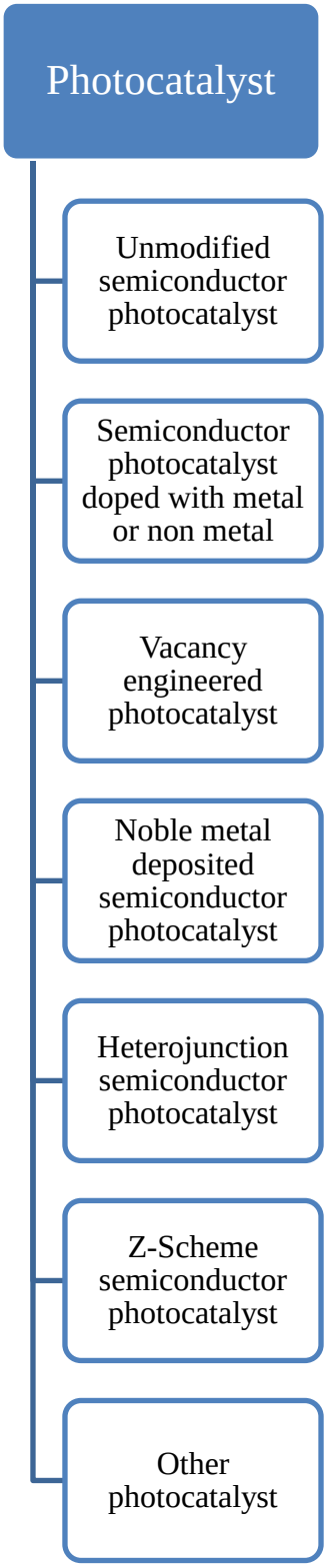

Fig 4: Different types of photocatalyst

(i) Unmodified semiconductor photocatalyst:

Unmodified semiconductor photocatalyst is a type of photocatalyst where pure metal is used as a photocatalyst without any modification of properties by adding several impurities. Graphitic carbon nitride (g-C_3N_4), WO_3, BiOX (X = F, Br, Cl and I) and other metal-free narrow bandgap (2.5-2.7 eV) semiconductors are popular visible light photocatalysts because they are easy to prepare, have high chemical stability, and have an efficient visible light response. This photocatalyst's VB potential is lower than the standard redox potentials of $OH^{\bullet}/H_2O$ and $OH^{\bullet}/OH^{-}$, limiting the generation of $OH^{\bullet}$ (Hong, Li, et al., 2016).It is not possible to make a single photocatalyst that has both good visible light response and high redox ability. A major limitation of pure unmodified photocatalyst is the rapid recombination of photogenerated e^{-}–h^{+} pairs (Xue et al., 2015). For that reason now a days the unmodified semiconductor photocatalyst is not generally directly used for the effective removal of organic pollutant, rather than it is modified by several methods like doping, adding nanoparticles, creating vacancy etc.

(ii) Semiconductor photocatalyst doped with metal or non metal:

Doping wide band-gap photocatalysts with metals (Sr, Co, Ti, Bi, Fe, etc.) and nonmetals (C, N, S, B, etc.) can narrow the band-gap, allowing visible light to pass through while also improving efficiency of e^{-}– h^{+} separation. TiO_2, ZnO, g-C_3N_4 have excellent photocatalytic activity towards the degradation of organic pollution but due to their wide band-gap they are not effective in visible range. By lowering the band gap energy of ZnO nanoparticles by doping and introducing impurities, they became more photocatalytically active over a wider range of wavelengths (UV to visible)(S. Sun et al., 2013). For enhancing the photocatalytic oxidation of organic dyes under UV and visible light irradiation, ZnO nanoparticles have been modified with different dopants consisting of N and S atoms (Shinde et al., 2012). N-doped ZnO showed 96.22% efficiency towards the removal of Methylene Blue (MB) dye under visible light irradaiation (Prabakaran & Pillay, 2019).In similar way it is observed that TiO_2/g-C_3N_4heterojuntion showed 90% efficiency towards the removal of Methyl Orange (MO) dye under visible light irradiation, which is increased to 99.8% for carbon-nitrogen-sulfer hetero atom doping (Z. Huang et al., 2021).

(iii) Vacancy Engineered photocatalyst:

Defect engineering, particularly vacancies, has a significant impact on the alteration of photocatalyst properties (Niu et al., 2018).Vacancy induction improves the electronic structure, inhibits electron hole recombination, and can even act as a specific reaction site, improving photocatalytic performance (Ding et al., 2018). It aids in the reduction of the semiconductor's band-gap energy, which increases the semiconductor's light-harvesting range. The creation of nitrogen vacancies in g-C_3N_4 can has been shown in recent studies to significantly improve the photocatalytic efficiency of bulk g-C_3N_4 (Ding et al., 2018; Niu et al., 2018; Paquin et al., 2015).In the recent past, oxygen vacancy induced photocatalyst synthesis is becoming a research hotspot because it enriches the electron trapping and active sites, which in turn enhance the charge carrier separation, absorption and activation ability for O_2 molecules(Y. Huang et al., 2014). Wang et al. have reported an oxygen vacancy induced $BiO_{2-x}/Bi_2O_{2.75}$ Z-scheme heterojunction, which has shown superior photocatalytic activity(Wang et al., 2019). Goud et al. analyzed surface oxygen vacancy facilitated Z-scheme MoS_2/Bi_2O_3 heterojunction towards the removal of Crystal Violet (CV) dye under visible light irradiation (Goud et al., 2020). In an another study by Khan et al. reported for surface oxygen vacancy CeO_2-Graphene nanostructure towards the degradation of organic dyes (Khan et al., 2017).

(iv) Noble metal deposited semiconductor photocatalyst:

The photocatalytic performance of a semiconductor is improved by depositing noble metals such as Pt, Pd, Au, Ag, Cu, and others as a surface modifier. Because of the Schottky barrier at the metal– semiconductor heterojunction, photo-induced electrons in the conduction band (CB) can transfer to metal deposits, which act as electron acceptors, whereas photo-induced holes can remain on the semiconductor surface in semiconductor–metal composites. As a result, electron and hole recombination can be avoided, and the photocatalytic efficiency can be increased (Sá et al., 2008). Pt deposited in TiO_2 showed a great removal efficiency of RhB under visible light irradiation (D. Zhang, 2012). Silver is one of the good noble metal widely used for improving photocatalytic activity of semiconductor. Mosavi et al. reported Ag deposited CdSe/Zeolite nanocomposite has about 90% efficiency towards the removal of MB dye under visible light

irradiation (Mosavi et al., 2021). In an another study Shi et al. reported Ag/AgBr deposited Ag/Br/ZnO nanocomposite showed almost 100% efficiency for removal of RhB dye under visible light irradiation (Shi et al., 2014). Shen et al. studied by using different noble metal Ag, Ru, Au, Pd, Pt and constructed CdS/M/TiO_2 Z-scheme photocatalyst (M = Ag, Ru, Au, Pd, and Pt) and observed the removal efficiency of MB dye under visible light irradiation & reported their degradation potential in order of Ag >Ru>Au >Pd>Pt (Shen et al., 2010).

(v) Heterojunction semiconductor photocatalyst:

Heterojunction photocatalysts are now widely used, and they are more effective in separating photogenerated e^-– h^+ pairs due to the combined beneficial effects of the individual semiconductors. In heterojunction semiconductor one n-type and another p-type semiconductor are combined. For type II heterojunction the VB & CB of one semiconductor is in higher level compared to the other semiconductor. A p-type and an n-type semiconductor can form a type II heterojunction, with the p-type semiconductor having higher band edge levels and work function values than the n-type. After contact, free e from the n-type semiconductor flows to the p-type semiconductor until equilibrium (EF) is reached, resulting in positively charged n-type and negatively charged p-type semiconductors at the heterojunction interface. As a result of band edge bending, an internal electric field is formed, which leads to the formation of a potential barrier. The internal electric field facilitates the transport of photogenerated e from the p-type CB to the n-type CB and photogenerated h+ from the n-type VB to the p-type VB with incident light, resulting in the e^-–h^+ pair separation. Copper sulfides (CuS), is a p-type semiconductor with a narrow band gap of 2.0 eV, it has strong absorption potential of visible light. But pure CuS has low photocatalytic activity because of the rapid recombination of photo-induced e^-– h^+ pair (Gao et al., 2017). Bismuth tungstate (Bi_2WO_6) nanosheets have weak visible-light response and recombine readily with photogenerated carriers. But formation Bi_2WO_6/CuS p-n heterojunction showed about 99% efficiency towards the removal of RhB dye under visible light irradiation(Mao et al., 2021). In another example we can observe that Zirconium oxide (ZrO_2) is a n-type semiconductor which has a wide band gap of (5 eV) it shows very less efficiency in visible light. Cerium oxide (CeO_2) is an-type semiconductor having a relatively narrow band gap

of 2.7. A combination of two semiconductors with different and gap level energies of type n-n junction showed exhibited better photocatalytic properties than single ones.

(vi) Z-Scheme semiconductor photocatalyst:

The natural photosynthetic process of water splitting inspired Z-schemes (Natarajan et al., 2018). Although the Z-scheme photocatalyst has the same band structure configuration as a heterojunction, the mechanism of charge carrier transfer is different. In comparison to traditional Type I and Type heterojunctions, the Z-scheme can effectively separate electrons and holes in different semiconductors while maintaining higher oxidation and reduction potentials for holes and electrons (Haijin Li et al., 2015). This exaction transfer mechanism promotes recombination of photogenerated e^{-}– h^{+} with weaker redox abilities, spatially separating and preserving photogeneratede^{-}– h^{+} with superior redox abilities for photocatalytic reactions (Q. Xu et al., 2018). Additionally, narrow band gap semiconductors can be used to construct Z-scheme systems, extending the light absorption range while maintaining the photocatalyst's high redox ability. The development of Z-scheme heterojunctions is a promising research area because it can improve light absorption and charge separation (Wang et al., 2019).Bulk g-C_3N_4 is a good photocatalyst with band-gap 2.7 eV but the photocatalytic activity is generally restricted by its limited charge-transfer capacity. For enhancement of photocatalytic activity Z-scheme heterojunction can be made, for that it is necessary to identify the semiconductor of suitable band structure. In this regard V_2O_5 semiconductor can be used to create the Z-scheme, which has several advantages including a narrow band gap, a wide range of light response, and chemical properties that are relatively stable(Yan & Liu, 2020). Hong, Jiang et al. used thermal polymerization to make a V_2O_5/g-C_3N_4 Z-scheme heterojunction composite and found that its efficiency in photocatalytic degradations of Rhodamine B (RhB) was significantly higher than that of V_2O_5 and g-C_3N_4 (Hong, Jiang, et al., 2016).

(vii) Other Photocatalyst:

In recent years nanocomposite photocatalyst are mostly in use they are basically the combination of multiple photocatalyst. These nanocomposites are not fall in the above mentioned categories but we can get idea about their charge transfer mechanism from the above categories. These nanocomposites are very much effective for degradation of synthetic dyes under visible light.

For examples Ag-based semiconductors such as AgX (X = Cl, Br, I), Ag_2CrO4, Ag_2MoO_4, $AgVO_3$, Ag_3PO_4, Ag_2CO_3, Ag_2WO_4, etc., are the promising candidate for photocatalysis as they respond to visible light efficiently due to their narrow band-gap. Among them Ag_2MoO_4 nanoparticle used widely in various applications such as photo-switch devices, gas-sensing, antimicrobial agents, ion-conducting glasses etc(Deb & Ghosh, 2011; Gouveia et al., 2014). Bi_2MoO_6 is an excellent photocatalytic agent in UV region but it is less active in visible region (Z. Zhang et al., 2021). Balasurya et al. prepared Bi_2MoO_6/Ag_2MoO_4 nanocomposite which shows 91.8% efficiency towards the removal of MB dye under visible light (Balasurya et al., 2021). Copper Selenide (CuSe), for example, is a p type semiconducting material with good electrical and optical properties and a larger surface area, but it is less efficient under visible light irradiation due to its wider band gap. Because of GO's excellent electron conduction property, the combination of CuSe and Graphene Oxide (GO) (CuSe/GO composite) reduces electron-hole pair recombination, resulting in higher photocatalytic activity of the semiconductor materials(Ata et al., 2018). Iqbal et al. prepared CuSe/GO nanocomposite and observed 89% efficiency towards the removal of MG dye in visible light (Iqbal et al., 2021). Similarly BPN & ZnAl-LDH nanocomposite (J. Yang et al., 2021)**,** TiO_2/PVA/cork nanocomposite (Mohamad Idris et al., 2021)**,** are recently discovered nanocomposites which shows great efficiency towards the removal of MB dye under visible light irradiation.

Photocatalytic degradation of dyes:

Conventional treatment process like chemical coagulation, electro coagulation, biological process, adsorption etc. are not able to completely remove the dyes as discussed above. Also these processes have several disadvantages like high cost, sludge production, hard to handle etc. For that advance oxidation process is used in removal of these dyes. Photocatalysis process is one of the advance oxidation processes, which can able to remove dye in efficient way. Basic mechanism of photocatalysis process is already discussed above. There are various types of photocatalysis like unmodified photocatalysis, Nobel metal deposited photocatalysis, vacancy

engineered photo catalysis, heterostructure photocatalysis, z scheme photocatalysis that also discussed in above chapter. TiO_2, ZnO, WO_3 etc are the most common semiconductor photocatalyst are use for pollution treatment but these photocatalyst have wide band gap and thus are ineffective to remove dyes in visible range. For that reason researchers are mostly focused on preparation of nanocomposite which is the composition of different type of material with semiconductor photocatalyst with gives great removal efficiency. The different literature and recent advancement regarding photocatalysis removal of dye under visible light irradiation are described in below as a chronological order.

Dongfang Zhang prepared titania nanoparticles and metallic platinum Pt/TiO_2 nanocomposites via a soft chemical reduction method for removal of RhB under visible light irradiation. The high efficiency of charge-pair separation due to the presence of deposited Pt serving as electron sinks to retard the rapid e^--h^+ couple recombination; the good photo absorption capacity in the visible light region; and the higher concentration of surface hydroxyl groups, which can effectively scavenge photogenerated valence band holes, can all be attributed to the Pt/TiO_2nanocomposite photocatalyst's superior visible light-driven photo The formation of $OH^\bullet$ as a reactive species that readily oxidises the organic dye molecule increases as holes accumulate on the catalyst surface (D. Zhang, 2012).

Shi et al. synthesized Ag/AgBr/ZnO composites using a two-step deposition precipitation method, followed by reduction under visible light irradiation to remove the RhB dye. Under visible light, Ag/AgBr/ZnO composites had significantly better photocatalytic activities for the degradation of RhB dye than pure ZnO. Synergetic effects such as increased visible light absorption, narrowed band gap, and effective separation of photogenerated electron-hole pairs are thought to be responsible for the increased photocatalytic activity. Furthermore, catalytic repetitive tests revealed that the Ag/AgBr/ZnO composite maintained good stability after 10 cycles, with activity decreasing slightly (Shi et al., 2014).

X. Liu et al., successfully synthesized a novel bi-functional Z-scheme heterojunction WO_3/g-$C_3N_4$with well-defined morphology by in-situ liquid phase process for the removal of MB under visible-light irradiation. It shows 95% removal efficiency in 90 min. The possible mechanism for the photocatalytic activity enhancement could be attributed to the formation of a Z-scheme

heterojunction system based on the active species trapping experiments. It is observed that $^{\bullet}O_2^-$ is the main reactive species for degradation of MB (X. Liu et al., 2017).

Prabakaran and Pillay used a hydrothermal method to make nitrogen doped zinc oxide nanoparticles with a cabbage-like morphology (N-ZnONCBs) as a photocatalyst for photocatalytic degradation of MB under UV and visible light. Under UV and visible light irradiation for 80 minutes and 50 minutes, respectively, the N-ZnONCB photocatalyst showed efficient MB degradation (98.6 percent and 96.2 percent). In this experiment, the dye was completely mineralized. The photo-stability and reusability of the N-ZnONCB catalyst were also investigated, with a percentage degradation rate of MB (93.2%) after four cycles. Both radicals $^{\bullet}O_2^-$ and $OH^{\bullet}$ have been shown to be good oxidizing agents that readily react with the MB molecule to produce CO_2, H_2O, Cl, SO_4^{2-} and NO_3^- as degradation products (Prabakaran & Pillay, 2019).

Arifin et al., reported the photocatalytic decomposition of MB over titania doped copper ferrite, $CuFe_2O_4/TiO_2$ photocatalyst synthesized via sol-gel method under visible light irradiation. It showed maximum efficiency 83.7 after 3 hours of irradiation at the optimum dose of 0.5 g/L. This photocatalyst facilitates the absorption of photons and reduces the recombination of electron hole pair by effective charge separation which improves the photocatalytic activity (Arifin et al., 2019).

Ghosh & Pal,reported the simple fabrication of a novel visible light active photocatalyst for the removal of MB in the presence of LED light by hydrothermally loading Bi_2O_3 nanoparticles on nitrogen vacant 2D g-C_3N_4 nanosheets. This enhanced the electron hole separation efficiency which improved the photocatalytic activity toward the degradation of MB. It shows 92% removal efficiency in 60 min (Ghosh & Pal, 2020).

El-Katori et al., synthesized an efficient and recyclable CdS/SnO_2 heterostructure for photocatalytic degradation of MB dye under UV and natural sunlight radiations. This photocatalyst enhanced the separation efficiency of the charge carrier and increasing the life time of the reactive radicals. It is observed that the electrons in conduction band and superoxide radicals are the predominant reactive species for photocatalytic activity. This exhibits an excellent photocatalytic stability and the catalyst retains 83 % of its reactivity after five

consecutive cycles revealing that there is no deterioration in the catalyst structure (El-Katori et al., 2020).

Ferreira et al., preparedreduced graphene oxide-zinc oxide (rGO-ZnO) composite by one-step method for removal of MB under visible light irradiation. It shows 98% removal efficiency in 90 min. The photocatalytic properties of ZnO, combined with the effective adsorption capacity of rGO sheets, make the composite highly efficient for water purification applications (Ferreira et al., 2020).

Chaudhary et al.,created novel graphene supported ternary nanocomposites (WO_3-ZnO@rGO) for the removal of MB under visible light irradiation using simple ultrasound assisted fabrication of WO_3-ZnO binary nanostructures over 2D rGO nanosheets. The photocatalytic efficiency of WO_3-ZnO@rGO was significantly improved by impregnation of WO_3-ZnO over rGO sheets with 94 percent dye removal in 90 minutes under visible light irradiation. By effectively separating and transferring photo-induced electron-hole pairs, the WO_3-ZnO@rGO improved photocatalytic efficiency. Furthermore, even after four recycling tests, WO_3-ZnO@rGO maintained its remarkable dye degradation efficiency. It's also been discovered that ROS participate in the degradation of MB in the order $OH^{\bullet} > h^{+} > {}^{\bullet}O_2^{-}$ (Chaudhary et al., 2020).

Lei et al., prepared Fe_3O_4@ZnO-RGO (RGO: reduced graphene oxide) composite with magnetic separation using the low-temperature hydrothermal method for removal of MB under visible light irradiation. Compared with the pure ZnO and Fe_3O_4@ZnO nanoparticles, Fe_3O_4@ZnO-RGO has a wider adsorption range for MB in visible light, and good photocatalytic activity and cyclic stability. Also, the unique structural characteristics of Fe_3O_4@ZnO-RGO enabled the separation of electron-hole pairs, which lead to its enhanced photocatalytic properties (Lei et al., 2020).

Using the citrate precursor method, Chahar et al. synthesized $Co_xZn_{(1-x)}Fe_2O_4$ (x= 0.0, 0.1, 0.2, 0.3, 0.4 and 0.5) for photocatalytic degradation of MB under visible light irradiation. An increase in cobalt concentration accelerated the degradation of MB. In 1 h of visible light irradiation, the

degradation efficiency reached a maximum (77%) for x = 0.5 and a minimum (65%) for x = 0.0. For photocatalytic degradation of MB, $OH^{\bullet}$ plays an important (Chahar et al., 2021).

Y. Zhang et al., synthesized 2D/2D Z-scheme heterostructure photocatalyst of BiOBr/TzDa covalent organic framework (COF) (BTDC) via a facile hydrothermal method for the removal of RhB/Cr(VI) mixture. Nearly 97% of total RhB and Cr(VI) in the mixture could be removed in 20 min and 40 min, respectively. It is observed by them that h^+ and $^{\bullet}O_2^-$ take crucial part in the degradation of RhB while $OH^{\bullet}$ plays a minor role, and the function of reactive species responsible for RhB degradation decrease in the sequence of $h^+ > {}^{\bullet}O_2^- > OH^{\bullet}$ (Y. Zhang et al., 2021).

Mosavi et al., examined for the removal of MB dye by Ag@CdSe/Zeoilte photocatalyst, prepared by Response Surface Methodology (RSM). According to their findings, [MB] = 7.17 mg/L, Ag@CdSe/Zeolite dosage = 0.03 g/50 mL, pH = 8, and t = 40 minutes resulted in 89.98 percent MB removal. They also observed that in alkaline medium MB readily reacts with OH^0 and converted to CO_2 gas and effectively removed from the solution (Mosavi et al., 2021).

Z. Huang et al., analyzed forremoval of MO dye by carbon-nitrogen-sulfur co-doped TiO_2/g-C_3N_4 Z-scheme heterojunction photocatalyst, prepared via one-step hydrothermal and calcinations methodsunder visible light irradiation. Under visible light irradiation, CNS- TiO_2/g-C_3N_4 Z-scheme heterojunction photocatalyst had excellent degradation performance (99.8%) when compared to pure TiO_2 and g-C_3N_4. It is observed by them that $^{\bullet}O_2^-$ & $OH^{\bullet}$ plays an active role in MO photocatalytic degradation process but h^+ plays a minor role (Z. Huang et al., 2021).

X. Zhang et al., analyzed for removal of MO dye from water by V_2O_5/P-g-C_3N_4Z-scheme heterojunction photocatalyst under the visible light irradiation. The results showed that the V_2O_5/P-g-C_3N_4 Z-scheme heterostructure degraded MO at the fastest apparent rate: 14.5 and 3.7 times faster than V_2O_5 and P-C_3N_4 when used separately. In just 105 minutes, they were able to achieve 90% efficiency. They also discovered that the primary active species in the photocatalytic degradation of MO were h^+ and $^{\bullet}O_2^-$ (Xinfei Zhang et al., 2021).

Ghattavi & Nezamzadeh-Ejhiehconstructed a double Z-scheme AgI/ZnO/WO_3 photocatalyst for removal of MB under visible light irradiation. This photocatalyst showed a lower electron/hole

recombination that favors the photocatalytic activity. It removes 85.2% of MB in 48.5 min. It was investigated that the photogenerated holes and hydroxyl radicals have the most essential roles in MB photo degradation by the composite (Ghattavi & Nezamzadeh-Ejhieh, 2021).

Asadzadeh-Khaneghah et al., synthesized g-C_3N_4 nanosheet/carbon dot/FeOCl (denoted as C_3N_4-NS/CD/FeOCl) nano-composites through a simple calcinations procedure for photo degradation RhB dyes under visible light irradiation. The outcomes demonstrated that 250 mL of RhB solution could be successfully removed in 60 min with 0.1 g of the optimum nanocomposite. It is observed by them that h^+, $OH^{\bullet}$, and $^{\bullet}O_2^-$ all contribute in the elimination reaction (Asadzadeh-Khaneghah et al., 2021).

Mao et al., synthesized Bi_2WO_6/CuS p-n heterojunction photocatalyst for the removal of Rhodamine B (RhB) dye under visible light irradiation. Approximately 98.8% of the RhB (10 mg/L) removed from a mixed solution within 105 min. Here photogenerated electrons/holes transferred to the surface of theBi_2WO_6/CuS and remove the RhB directly. Bi_2WO_6/CuS can be applied over a wide pH range (2–6) with strong photocatalytic activity for removal of RhB (Mao et al., 2021).

Noman et al., synthesized p-n CuO/CeO_2ZrO_2 heterojunction photocatalyst by the auto solution combustion method for the removal of Methelene Blue (MB) dye under visible light irradiation. This shows 98% removal efficiency in 3hr. They observed that $OH^{\bullet}$, $^{\bullet}O_2^-$, h^+ plays main role in photocatalytic degradation process. Whereas the H_2O_2 did not play an important role for degradation of MB by CuO/CeO_2ZrO_2 (Noman et al., 2021).

Balasurya et al., examinedfor the removal of Methelene Blue (MB) dye with the help of Bi_2MoO_6-Ag_2MoO_4 nanocomposite heterojunction photocatalyst prepared via facile synthesis method under visible light irradiation. Bi_2MoO_6-Ag_2MoO_4 nanocomposite exhibited 91.8% degradation efficiency obtained after 6th cycle which was highly effective than individual Ag_2MoO_4 (54.66%) and Bi_2MoO_6 (58.6%). It is also reported by them that this heterojunction can prevent the recombination of e^-/h^+ pair and enhance the photocatalytic degradation process. $OH^{\bullet}$ plays the major role in photocatalytic degradation of MB dye (Balasurya et al., 2021).

Iqbal et al., analyzed the photocatalytic activity of composite of copper selenide nanoparticles and graphene oxide (CuSe/GO) for removal of Methyl Green under solar light irradiation. They

made CuSe using a hydrothermal method and GO using a modified Hummer's method, and then made a CuSe/GO composite. In 45 minutes, the CuSe/GO removed 89 percent of the MG (Iqbal et al., 2021).

Yang et al., reported a new kind of environmental-friendly nanocomposite consisting of ZnAl-layered double hydroxides (LDH) and black phosphorus nanosheets BPNs, obtained by electrostatic self-assembly method for removal of MB under visible light irradiation. The ZnAl-LDH and BPNs, nanocomposite photocatalyst shows the 99% degradation of MB in 80 min. The improvement of photocatalytic performance is mainly because BPNs provide an additional transfer channel of electrons and holes. $OH^{\bullet}$ is mainly responsible for the degradation of MB whereas $^{\bullet}O_2^-$ is not the main species, but it further converted to $OH^{\bullet}$ through the reductive paths ($^{\bullet}O_2^- \rightarrow H_2O_2 \rightarrow OH^{\bullet}$) (J. Yang et al., 2021).

Mohamad Idris et al.,reported the titanium dioxide nanoparticles (TiO_2 NPs) / polyvinyl alcohol (PVA) / cork nanocomposite a floating photocatalyst, where cork act as a on the floating substrate employing polyvinyl alcohol (PVA) as a binder to anchor TiO_2 NPs on the surface of the cork. They used this photocatalyst for removal of MB under visible light irradiation. It is examined that this nanocomposite possessed a slower recombination rate of electron-hole pairs as compared to anatase TiO_2. At the optimal mole ratio of TiO_2/PVA (1:8), the TiO_2/PVA/cork floating photocatalyst degraded at 98.43% of methylene blue (MB) under a visible light source in 120 min. The superior photodegradation performance for MB was mainly controlled by the reactive oxygen species of the superoxide radical ($^{\bullet}O_2^-$). The degradation kinetics of MB followed the first-order kinetics (Mohamad Idris et al., 2021).

CHAPTER 3

MATERIALS AND METHODS

3.1 MATERIALS

The synthetic solution of MB of Merck is prepared which is used as the organic pollutant. Bismuth Nitrate ($Bi(NO_3)_3.5H_2O$), Sodium Molybdate ($Na_2MoO_4.2H_2O$), Potassium Nitrate (KNO_3), Sodium Nitrate ($NaNO_3$) are of Merck are used to prepare the Bi_2MoO_6. For the synthesis of g-C_3N_4, Urea of Merck was used. Millipore water was used throughout the study.

3.2 PHOTOCATALYST SYNTHESIS

3.2.1 SYNTHESIS OF Bi_2MoO_6

Bi_2MoO_6 was prepared by molten salt method following a recent study (G. Yang et al., 2020). Typically, Bismuth Nitrate ($Bi(NO_3)_3.5H_2O$) of 4 gm and Sodium Molybdate ($Na_2MoO_4.2H_2O$) of 1 gm were used for maintaining the molar ratio of Bi:Mo = 2:1 as the precursors and grinded for about 15 mins in an agate mortar. Subsequently, KNO_3 and $NaNO_3$ salt mixtures with a weight ratio of KNO_3: $NaNO_3$ = 1:1 were taken as the co-solvent. Molten salt each of 20 gm is taken and a total wt of raw material and molten salt of 45 gm is made so that the weight ratio of raw material to molten salt becomes 1:8. After being grinded for over 30 mins, the mixtures including raw materials and molten salts were placed in an alumina crucible and then calcined at a temperature of 400°C in a muffle furnace for duration of 10 h. After the molten salt reaction, the as-obtained catalysts were washed for at least three to four times with deionized water to remove the molten salts, respectively, and the resultant products were dried at 80°C for 24 h for further experiment. The schematic diagram for preparation of Bi_2MoO_6, shown in below Fig. 5.

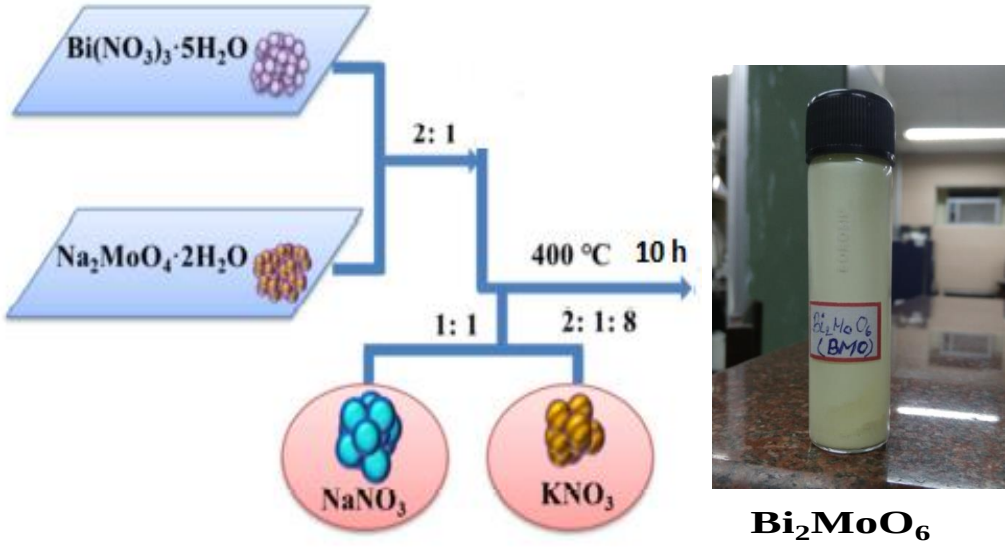

Fig 5: Schematic diagram for preparation of Bi_2MoO_6

3.2.2 SYNTHESIS OF g-C_3N_4 NANOSHEETS

Following a prior study, the g-C_3N_4 nanosheets were made by thermal oxidation etching of bulk g-C_3N_4 in air(Niu et al., 2012). Bulk g-C_3N_4 was produced by calcining urea at 550°C for four hours in the air. To make g-C_3N_4 nanosheets, the product was ground and calcined at 500°C for two hours. The schematic diagram for preparation of Bi_2MoO_6 is shown in below Fig. 6.

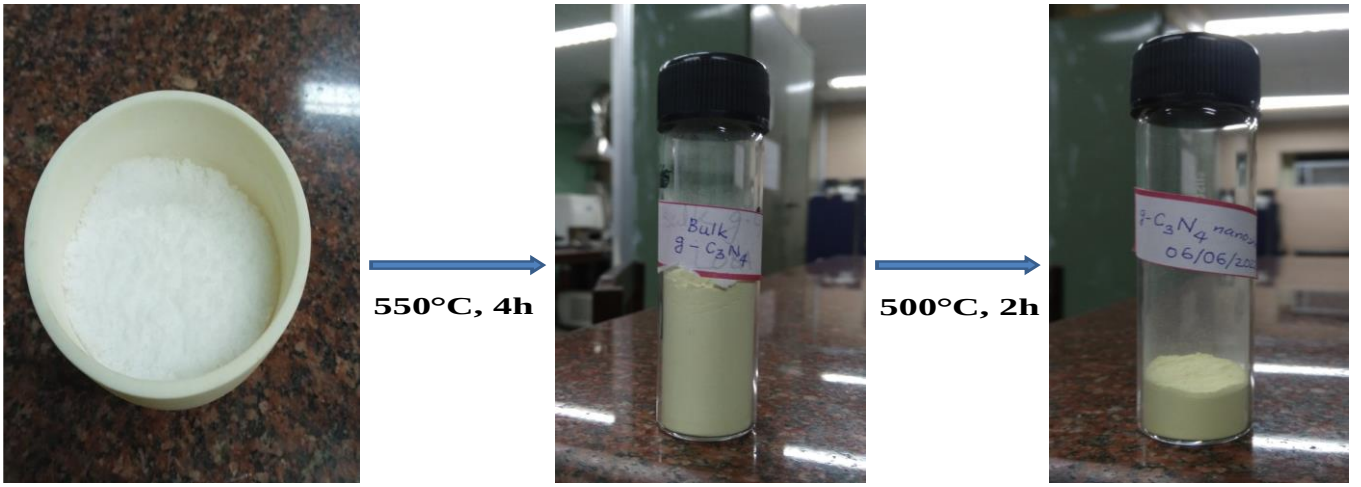

Fig 6: Schematic diagram for preparation of g-C_3N_4 nanosheets from Urea

3.2.3 SYNTHESIS OF g-C_3N_4/Bi_2MoO_6 NANOCOMPOSITE

The hydrothermal method was used to make the Bi_2MoO_6/g-C_3N_4 nanocomposite. Initially, 100 mg of Bi_2MoO_6 and a specific amount of g-C_3N_4 nanosheets were added to 40 ml deionized water, followed by 30 minutes of sonication, and then the 100 mg of g-C_3N_4 nanosheets and a specific amount of Bi_2MoO_6 were added to 40 ml deionized water, followed by 30 minutes of sonication. The resulting mixtures were then transferred to a 50 mL Teflon-lined hydrothermal autoclave and treated for 24 hours at 160°C. The products were thoroughly washed and dried at 80°C for 24 hours after the hydrothermal treatment. The synthesis protocol of Bi_2MoO_6/g-C_3N_4 nanocomposites is presented in below figure no. 7. The amount of g-C_3N_4 nanosheets was varied to obtain g-C_3N_4/Bi_2MoO_6nanocomposites having mass ratios of 10, 20, 30 and 40%, designated as 10g-C_3N_4/Bi_2MoO_6, 20g-C_3N_4/Bi_2MoO_6, 30g-C_3N_4/Bi_2MoO_6 and 40g-C_3N_4/Bi_2MoO_6 respectively which is denoted by the symbol of **A, B, C, D** respectively. The amount of Bi_2MoO_6 nanosheets was varied to obtain Bi_2MoO_6/g-C_3N_4 nanocomposites having mass ratios of 10, 20, 30 and 40%, designated as 10Bi_2MoO_6/g-C_3N_4, 20Bi_2MoO_6/g-C_3N_4, 30Bi_2MoO_6/g-C_3N_4 and

40Bi_2MoO_6/g-C_3N_4 respectively which is denoted by the symbol of **E, F, G, H** respectively. The schematic diagram for preparation of Bi_2MoO_6 is shown in below Fig. 7.

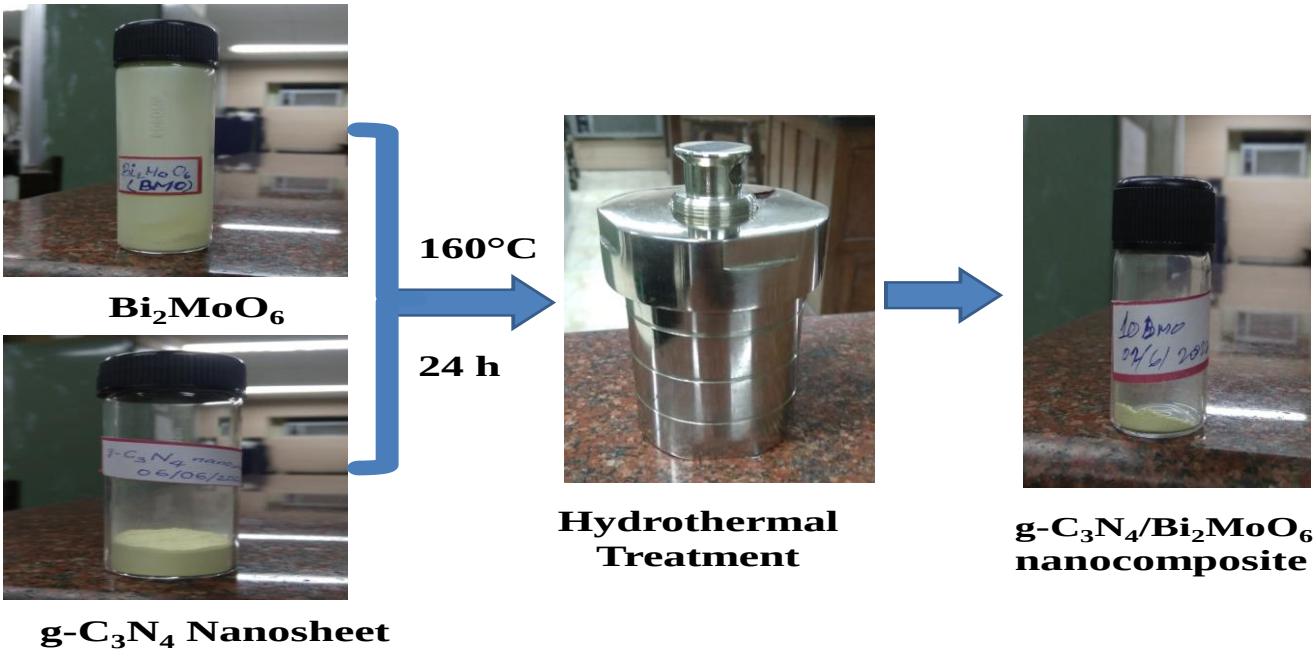

Fig 7: Schematic diagram for preparation of Bi_2MoO_6/g-C_3N_4 nanocomposite

3.3 CHARACTERIZATION

UV-Vis DRS Characterization of as-synthesized materials is done to determine the band gap of the as-synthesized. Using the data obtained from the experiment the photocatalytic performance of the materials is determined.

3.4 PHOTOCATALYTIC EXPERIMENT

The photocatalytic efficiency of the as-synthesized Bi_2MoO_6/g-C_3N_4 nanocomposites was evaluated by degrading MB under visible LED light (20-W, Philips, India) irradiation. Typically, a 10 mg dose of photocatalyst was mixed with 10 ml of MB (20 mg/l) in a glass beaker. A magnetic stirrer was used to stir the mixture at 500 rpm for 30 minutes in the dark to achieve adsorption–desorption equilibrium between the catalyst and MB. The photocatalytic reaction under visible light irradiation followed. The supernatant was filtered using a 0.22 mm syringe

filter after the photocatalytic reaction was completed, and the MB concentration was determined using a visible spectrophotometer (SYSTRONICS VISIBLE-SPECTRO 105) at a wavelength of 665 nm. The MB removal efficiency was determined using the below Eq. 9:

$$R\ (\%) = \frac{C_0 - C_t}{C_0} \times 100 \qquad (9)$$

Where "R" is the percentage removed of MB at the time "t". C_0 and C_t are the initial and final MB concentrations respectively.

3.5 RADICAL SCAVENGING EXPERIMENT

To scavenge superoxide radicals (O_2^{0-}), holes (h^+) and, hydroxyl radicals (OH^0), radical scavengers such as benzoquinone (BQ), ethylenediamine tetraacetic acid disodium salt (EDTA-2Na), and isopropanol (IPA) were used. The concentrations of BQ, EDTA-2Na, and IPA were 0.25 mM, 1 mM, and 1 mM, respectively. Photocatalytic degradation experiments were carried out in the same way as before, but with the addition of scavengers to the suspensions beforehand.

3.6 COD DETERMINATION EXPERIMENT

COD determination experiment is done by closed reflux colourimetric method. In this method firstly the standard absorbance curve of COD is determined using the spectrophotometer. For determination of standard COD curve the standard KHP (Potassium Hydrogen Pthalate) solution is of different concentration is made along with $K_2Cr_2O_7$ solution and Ag_2SO_4 solution is also prepared. 2.5 ml of KHP solution of different concentration along with 1.5 ml of $K_2Cr_2O_7$ solution and 3.5 ml of Ag_2SO_4 solution is mixed and heated at 150°C for 2 h in closed reflux. Then the sample is cooled and measured the absorbance value with respect to the different concentration of KHP. Following the creation of the standard curve, the MB sample is used in

place of KHP, and the respective COD is determined. The closed reflux setup is shown in below Fig. 8.

Fig 8: Closed reflux setup for determination of COD

CHAPTER 4

RESULTS AND DISCUSSION

4.1 CHARACTERIZATION OF MATERIALS

4.1.1 UV-Vis DRS

A photocatalyst's optical properties have a significant impact on its performance (Majumdar et al., 2021). Figures 9 and 10 show the UV–visible DRS and Tauc plots of Bi_2MoO_6, g-C_3N_4, and 10Bi_2MoO_6/g-C_3N_4. According to the DRS, the absorption edges of Bi_2MoO_6, g-C_3N_4 is around 490 nm, but the absorption edge of 10Bi_2MoO_6/g-C_3N_4 showed a bath chromic shift. The Tauc plots yielded bandgap energies (Eg) of Bi_2MoO_6 and g-C_3N_4 of 2.86 and 2.88, respectively. Thus, the increased absorption in the visible light range, and thus the increased photocatalytic efficiency of 10Bi_2MoO_6/g-C_3N_4, could be attributed to the synergistic effect of Bi_2MoO_6 and g-C_3N_4 nanosheets. Previous studies estimated the conduction band (CB) potential values of Bi_2MoO_6 and g-C_3N_4 (vs. NHE) from Mott-Schottky plots to be 0.45 eV (Opoku et al., 2018) and -1.2 eV (G. Xu et al., 2018), respectively. The value of valence band (VB) potential of Bi_2MoO_6 and g-C_3N_4 were calculated by the Eq. (10)

$$E_{vb} = E_g + E_{cb} \quad (10)$$

Where, E_{VB} and E_{CB} denote the VB and CB potential respectively. As a result, the calculated valence band (VB) potentials of Bi_2MoO_6 and g-C_3N_4 are +3.31 and +1.68 eV, respectively.

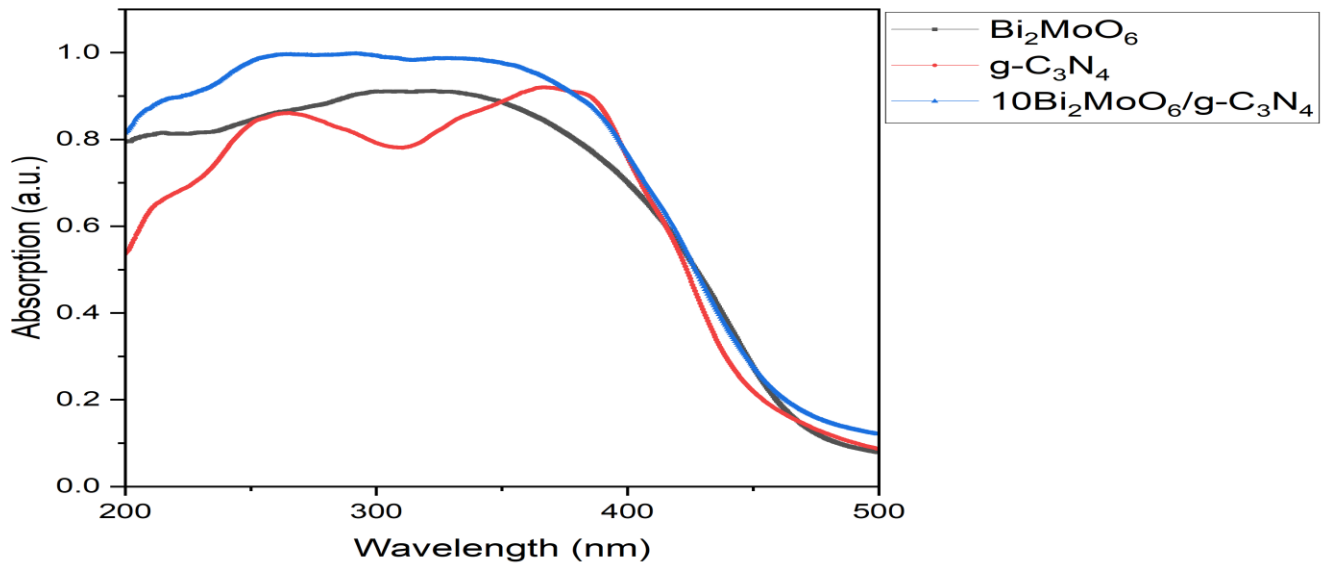

Fig 9: UV-Vis absorbance spectra of Bi_2MoO_6 , g-C_3N_4 and 10Bi_2MoO_6/g-C_3N_4 photocatalyst

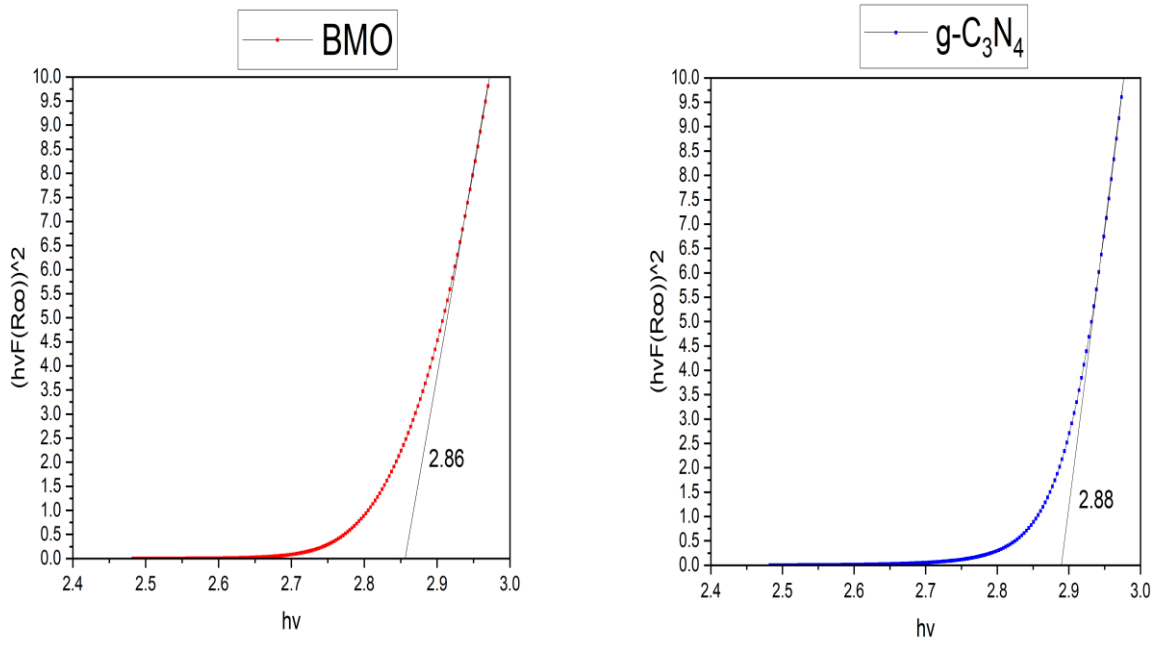

Fig 10: Tauc plot of Bi_2MoO_6 and g-C_3N_4

4.1 PHOTOCATALYTIC ACTIVITY

Figure 11 shows the photocatalytic activity of all the catalysts. MB is degraded by 11 percent in 10 minutes in the absence of catalysts, after which a very small change in photo-degradation is observed, reaching up to 16 percent over the course of 60 minutes, indicating that MB is relatively stable under visible light irradiation. Bi_2MoO_6 and g-C_3N_4 nanosheets degraded only 50.3% and 42.4% of MB within 60 min, respectively. The nanocomposite **A, B, C, D** shows only 34.5%, 42.06%, 36.97%, 36.77% MB removal efficiency respectivelybut a significant enhancement of photocatalytic efficiency for the degradation of MB was observed by the nanocomposite **E** which shows a degradation efficiency of 92.45% towards MB in 60 min. Similarly the degradation efficiency by the nanocomposite **F, G, H** are also determined which shows the MB degradation efficiency of 80.28%, 76.68% and 74.66% respectively. The slope of the "$\ln(C/C_0)$" vs "t" curve gives us the "k" value, and the results from MB degradation experiments were fitted in the linear form of pseudo first-order kinetics equation ($C = C0.e^{-kt}$) to get insightful information on the reaction kinetics. The R^2 values in Fig. 12 showed that the experimental results were consistent with the pseudo first-order kinetic equation. It's also worth noting that the apparent first-order rate constant (k) value of E nanocomposite is the highest (0.027 min^{-1}) among all nanocomposites, and it's 13.5 and 3.8 times higher than that of pristine Bi_2MoO_6 and g-C_3N_4 respectively.

For finding the optimum dose of photocatalyst three same solution of MB of 20 ppm is taken and treated by **E** nanocomposite in the dose of 0.5 g/l, 1 g/l, and 1.5 g/l respectively under same 20W visible LED light irradiation. The removal efficiency is shown by the graph in Fig. 13. From the graph it is clearly observed that by the photocatalyst dose of 0.5 g/l MB is removed upto 71% in 60 min. However a significant amount of increment of removal efficiency to 92.45% by the photocatalyst dose of 1 g/l. After that further increase in dose of photocatalyst to 1.5 g/l does not cause significant change of removal efficiency (93.46%). So from that experimental result it can by obviously said that 1 g/l is the optimum dose of photocatalyst **E** nanocomposite for removal of MB solution of 20 ppm concentration under 20W visible LED light irradiation. The Batch experiment and the initial and final concentration of MB using dose 1 g/l is shown in below Fig. 14 and Fig. 15.

The comparison between different recent literature of MB degradation using nanocomposite photocatalyst and this study is shown in below Table 3.

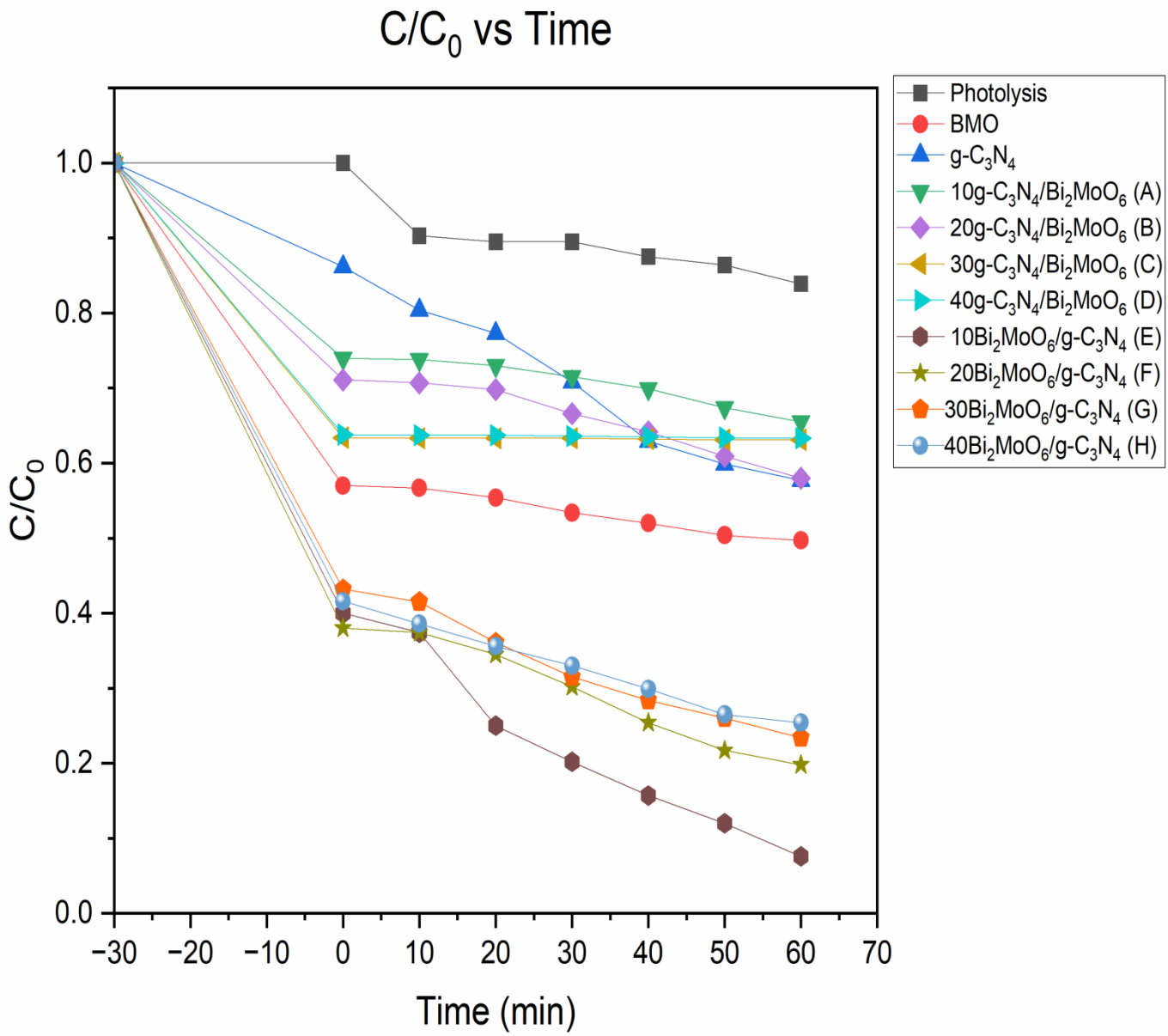

Fig 11: Photocatalytic degradation efficiency with respect to time using different photocatalysts

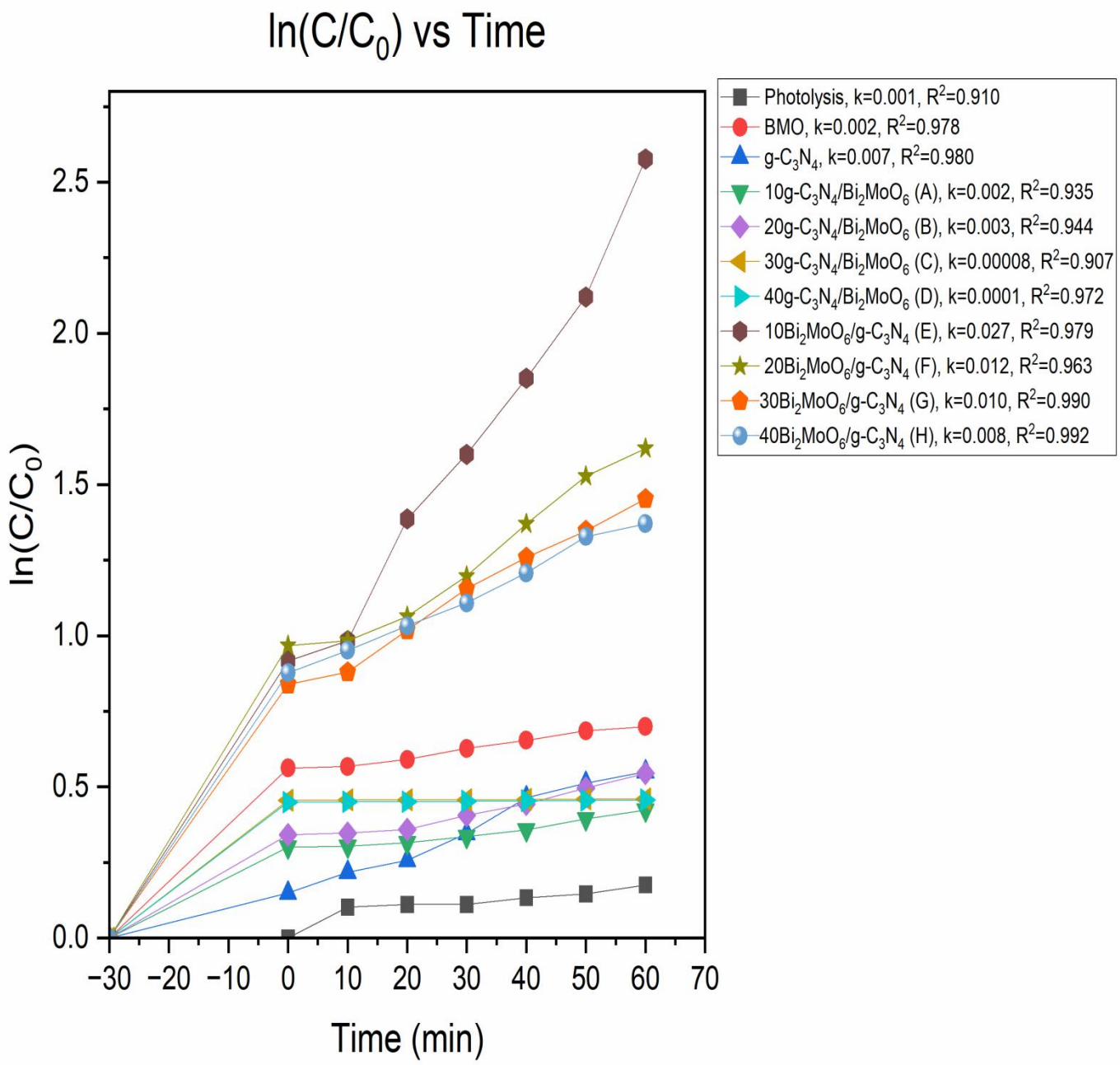

Fig 12: Pseudo first order reaction kinetics of different nanocomposites towards MB (20 mg/l) degradation

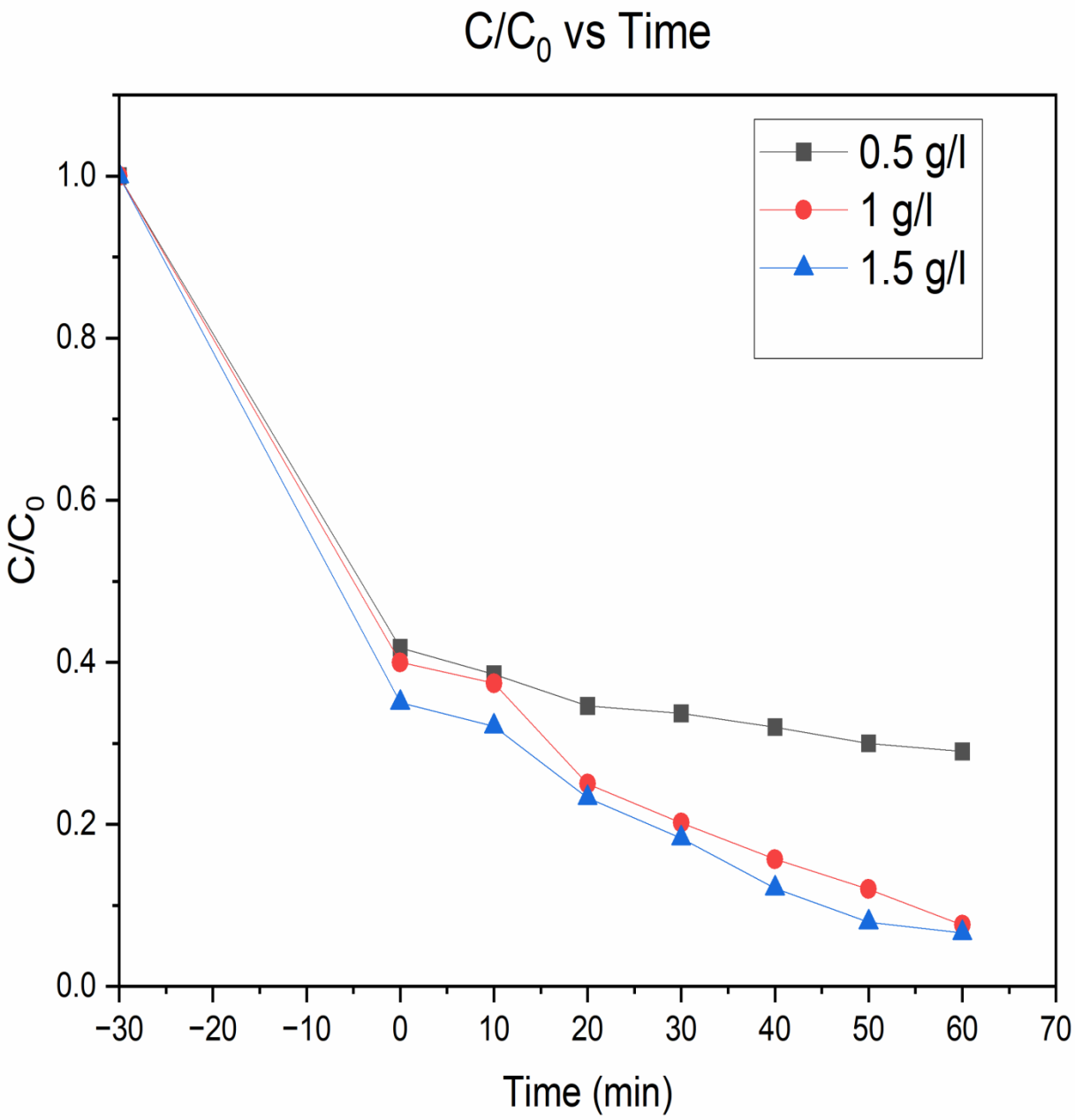

Fig 13: Dose variation of $10Bi_2MoO_6/g\text{-}C_3N_4$ (E) nanocomposite for determining the optimum dose towards MB (20 mg/l) degradation

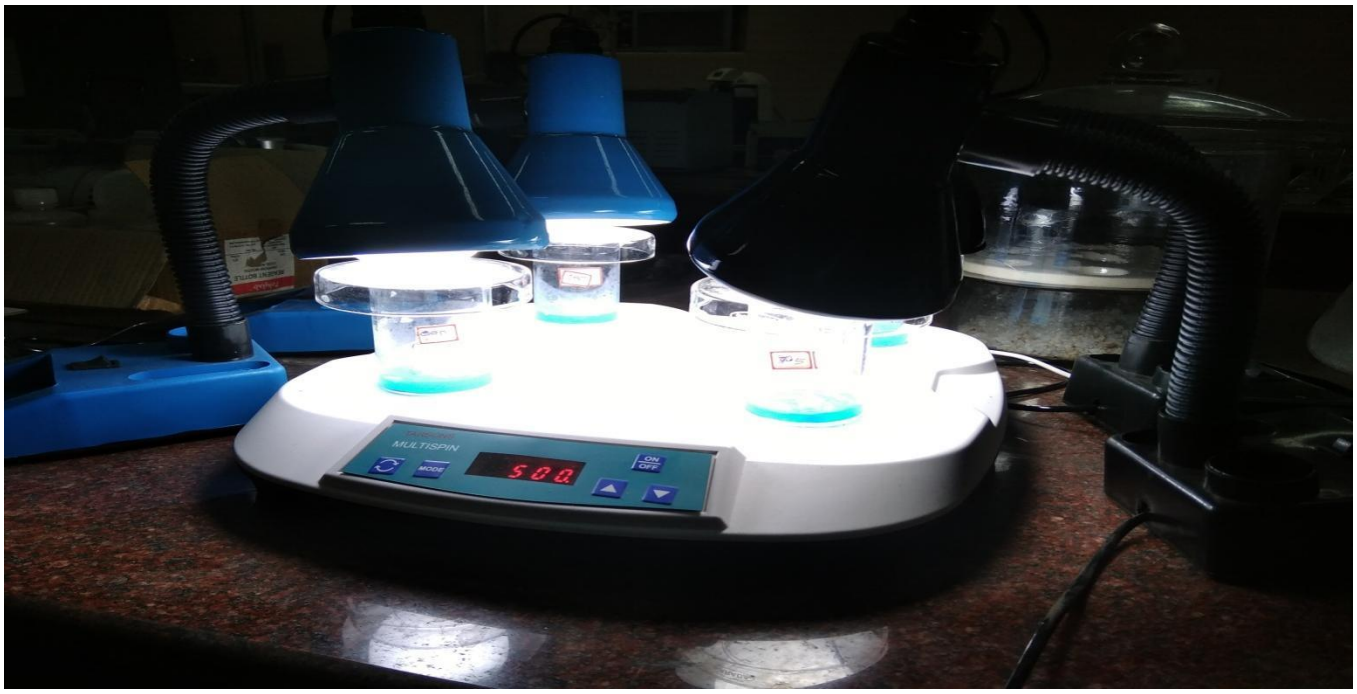

Fig 14: Batch experiment for removal of MB using as synthesized photocatalyst under 20W LED light irradiation

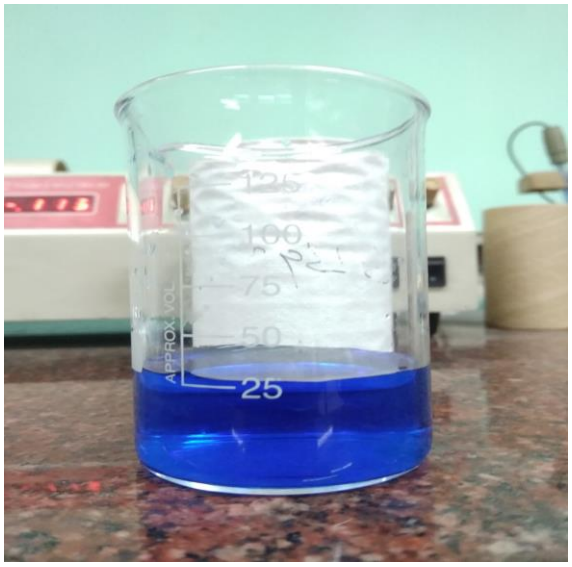

Initial MB solution before application of photocatalyst

Final MB solution after 1 h 20W LED light irradiation

Fig 15: Initial and final solution of MB under 1 g/l of photocatalyst dose in presence of 20W LED light

Table 3: Summary of the recent literature on photocatalytic MB degradation

Photocatalyst	Photocatalyst doses (g/l)	MB Concentration (mg/l)	Light Source	% Degradation/time (min)	Reference
$WO_3/g\text{-}C_3N_4$	0.5	50	300 W Xenon lamp	95%, 90 min	(X. Liu et al., 2017)
WO_3-ZnO@rGO	0.2	5	200 W tungsten filament lamp	94%, 90 min	(Chaudhary et al., 2020)
$AgI/ZnO/WO_3$	3.8	7	100 W tungsten filament lamp	85.2%, 48.5 min	(Ghattavi & Nezamzadeh-Ejhieh, 2021)
$CuFe_2O_4/TiO_2$	0.5	20	500 W Xenon lamp	83.7%, 3 hr	(Arifin et al., 2019)
Ag@CdSe / Zeoilte	0.6	7.17	300 W tungsten halogen lamp	89.98%, 40 min	(Mosavi et al., 2021)
BPN and ZnAl-LDH	1	20	300 W xenon lamp	99%, 80 min	(J. Yang et al., 2021)
$Bi_2MoO_6/g\text{-}C_3N_4$	1	20	20W LED lamp	92.45%, 60 min	**This study**

4.2 RADICAL SCAVENGING EXPERIMENT AND PHOTOCATALYTIC MECHANISM

To observe the primary reactive species causing MB degradation, several radical scavenging studies were carried out. Figure 16 depicts the study's results. BQ and IPA significantly reduce degradation efficiency, showing that $^{\bullet}O_2^-$ & $OH^{\bullet}$ are the primary reactive species in this investigation. The addition of EDTA-2Na results in a minimal drop in degradation efficiency, demonstrating that h+ has no direct effect on the breakdown of MB by "**E**" nanocomposite. As a result, ROS contribute in the order ($^{\bullet}O_2^-$> $OH^{\bullet}$>h^+) to the degradation of MB.

A tentatively probable mechanism for visible light photocatalytic water splitting and decomposition efficiency of the heterojunction is proposed based on the band positions result (Fig. 17). Photo-induced charge carriers are produced by both the semiconductors of g-C_3N_4 and Bi_2MoO_6 under visible light irradiation. When g-C_3N_4 and Bi_2MoO_6 form a conventional electron–hole separation process, the electrons accumulated in the CB of g-C_3N_4 tend to excite the CB of Bi_2MoO_6, because the CB position of g-C_3N_4 is more negative than Bi_2MoO_6. Meanwhile, under simulated visible light, the holes in the VB of Bi_2MoO_6 will migrate to the VB of g-C_3N_4, because the VB position of Bi_2MoO_6 is more positive than the g-C_3N_4 sheet. The heterojunction then forms a type-II staggered band alignment, which aids in the separation and transfer of photo induced electrons and holes. However, because the photo induced electrons on the CB of Bi_2MoO_6 are less negative than the potential required for O_2 generation ($O_2/^{\bullet}O_2^-$ = -0.33 eV vs NHE), they are unable to convert O_2 into superoxide ($^{\bullet}O_2^-$) radical anion. Furthermore, the VB potential of 1.68 eV for g-C_3N_4 is lower than the $H_2O/OH^{\bullet}$ redox potential (2.68 eV vs. NHE), indicating that the photo-induced holes accumulated on the VB of g-C_3N_4 are unable to oxidise the adsorbed water molecules to form an $OH^{\bullet}$ radical. As a result, if the photogenerated electrons and holes in the Bi_2MoO_6/g-C_3N_4 heterostructures are separated and transferred using the conventional hetero-junction process, the formation of $OH^{\bullet}$ and $^{\bullet}O_2^-$ ROS is not favourable, resulting in lower photo activity for pollutant degradation. As a result, the photo degradation activity of the Bi_2MoO_6/g-C_3N_4 heterojunction was lower.

Based on the foregoing discussion, it is suggested that the Z-scheme charge transfer system used by the Bi_2MoO_6/g-C_3N_4 heterostructures be used instead of the conventional system to account for the heterostructures' improved photocatalytic performance (Fig. 18).

The photo induced electrons in the Bi_2MoO_6 conduction band migrate to the valence band of the g-C_3N_4 sheet in the direct Z-scheme charge transfer mechanism. The surrounding water molecules can be oxidized into $OH^{\bullet}$ radicals by the more positive VB potential of Bi_2MoO_6 (3.31 eV) compared to the $H_2O/OH^{\bullet}$ potential. In addition, O_2 can be reduced to produce the reactive $^{\bullet}O_2^-$ radical anion due to the g-C_3N_4 sheet's CB potential, which is more negative (-1.20 eV) than the $O_2/^{\bullet}O_2^-$ potential. When compared to isolated Bi_2MoO_6 photocatalysts, heterostructures may exhibit higher reduction/oxidation ability due to higher levels of $^{\bullet}O_2^-$ and $OH^{\bullet}$ radical generation. This will enhance the photocatalytic activity. As a result, the degradation of the pollutant is caused by $^{\bullet}O_2^-$ and $OH^{\bullet}$ radicals. This implies that, as shown in equations 11 through 14, several pollutants in the water matrices can be degraded by reactive $^{\bullet}O_2^-$ and $OH^{\bullet}$ radicals with high activity.

$$g\text{-}C_3N_4 + Bi_2MoO_6 + h\nu \rightarrow g\text{-}C_3N_4(e^-) + Bi_2MoO_6(h^+) \quad (11)$$

$$g\text{-}C_3N_4\ (e^-) + O_2 \rightarrow {}^{\bullet}O_2^- \quad (12)$$

$$Bi_2MoO_6\ (h^+) + H_2O \rightarrow OH^{\bullet} + H^+ \quad (13)$$

$$OH^{\bullet}, {}^{\bullet}O_2^- + \text{pollutant} \rightarrow CO_2 + H_2O + \text{by products} \quad (14)$$

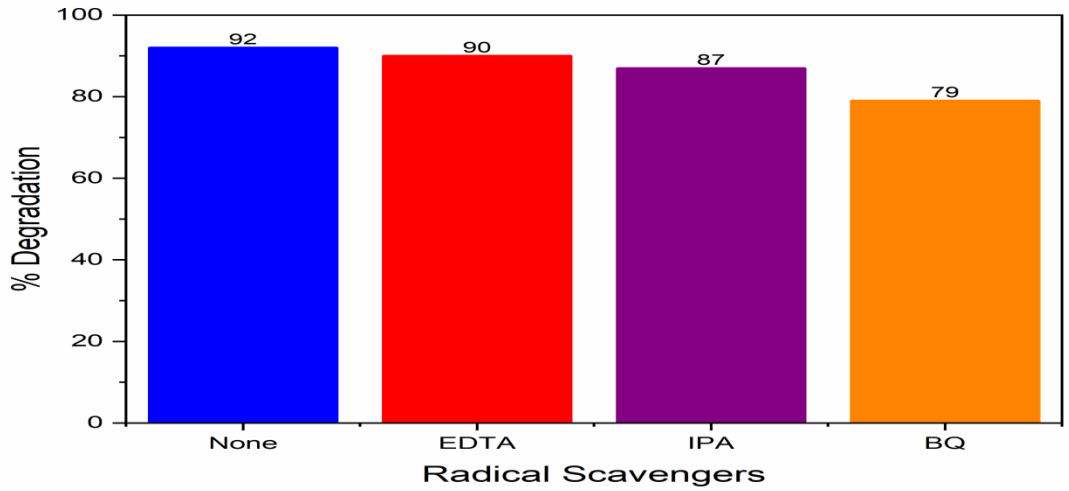

Fig 16: Photocatalytic degradation efficiency of 10Bi_2MoO_6/g-C_3N_4 nano-composites towards MB influenced by radical scavengers

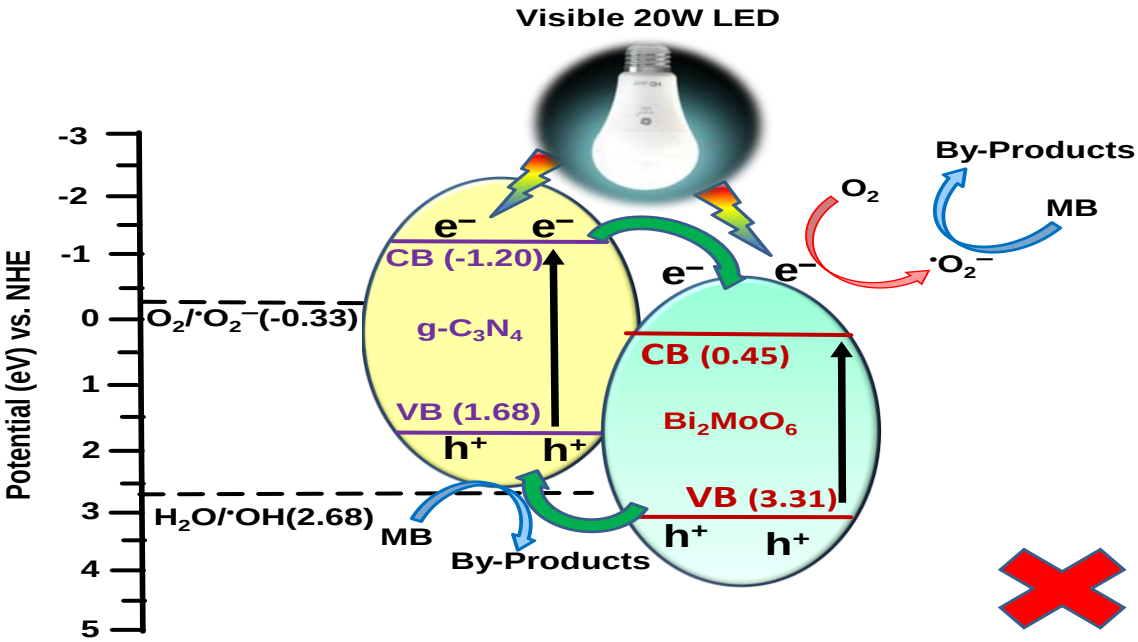

Fig 17: Photocatalytic Proposed hetero-junction charge transfer mechanism for the photocatalytic activity over 10Bi_2MoO_6/g-C_3N_4 nanocomposite.

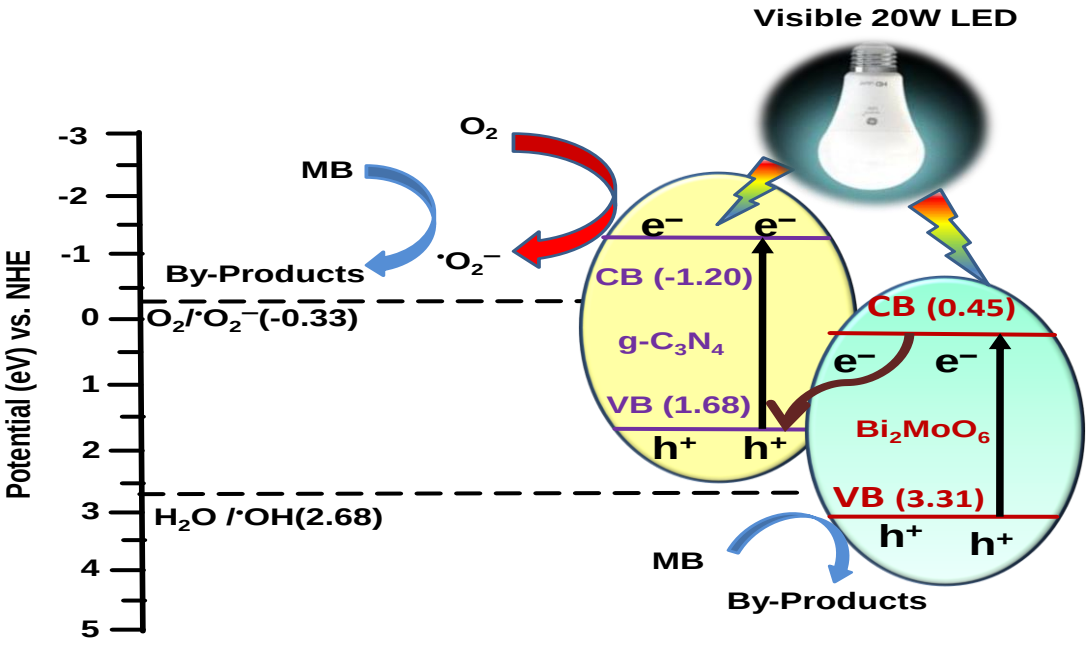

Fig 18: Proposed Z-scheme charge transfer mechanism for the enhanced photocatalytic performance over 10Bi_2MoO_6/g-C_3N_4 nanocomposite.

4.3 DETERMINATION OF COD REMOVALEFFICIENCY

COD removal efficiency can be determined by the below equation Eq. 10.

$$E\ (\%) = \frac{COD_i - COD_f}{COD_i} \times 100 \qquad (14)$$

Here "E" is the COD removal efficiency.COD_i&COD_f is the initial COD of MB solution before application of photocatalyst and final COD of MB solution treated by photocatalyst under 20W LED light irradiation. Both the COD of the solution is determined by closed reflux colourimetric method where firstly standard curve of COD is drawn using standard KHP solution then the COD of this MB solution is determined using that standard curve. Initial and final COD is found of 13 mg/l and 1 gm/l respectively. So using this above equation (10) we got a COD removal efficiency of 92%. So from this experiment we can conclude that this photocatalyst are able to remove 92% COD from solution.

CHAPTER 5

CONCLUSIONS

A hydrothermal method was used to successfully synthesize novel $10Bi_2MoO_6/g\text{-}C_3N_4$ nanocomposites. Its photocatalytic effectiveness for MB degradation under visible light has been reported. The optimized $10Bi_2MoO_6/g\text{-}C_3N_4$ nanocomposite, which was 1.84 and 2.18 times more efficient than pristine Bi_2MoO_6 and $g\text{-}C_3N_4$, respectively, under the 60 min of visible 20W LED light irradiation, achieved the maximum MB degradation efficiency (92.45 percent). The $10Bi_2MoO_6/g\text{-}C_3N_4$ nanocomposite showed the highest pseudo first order rate constant for MB degradation (0.027 min^{-1}). In comparison to pure Bi_2MoO_6 and $g\text{-}C_3N_4$, the $10Bi_2MoO_6/g\text{-}C_3N_4$ nanocomposite had higher photocatalytic efficiency because of its larger surface area, absorption of visible light, and separation of electron-hole pairs. Furthermore, the radical scavenging experiments proved that the main reactive species that cause MB to degrade over the $10Bi_2MoO_6/g\text{-}C_3N_4$ nanocomposite are $^{\bullet}O_2^-$ & $OH^{\bullet}$. Based on radical scavenging experiments and energy band structures, a Z-scheme heterojunction photocatalytic mechanism has been suggested. During the photocatalytic degradation of MB, the as-prepared $10Bi_2MoO_6/g\text{-}C_3N_4$ nanocomposite also displays a 92 percent COD removal efficiency. As a result, the current study illustrates the synthesis of a novel and effective photocatalyst for the low-cost, energy-efficient, visible light-assisted treatment of dye pollutants, which will encourage the synthesis of additional photocatalysts of a like nature for environmental remediation.

REFERENCES

Abid, M. F., Zablouk, M. A., & Abid-Alameer, A. M. (2012). Experimental study of dye removal from industrial wastewater by membrane technologies of reverse osmosis and nanofiltration. *Journal of Environmental Health Science and Engineering*, *9*(1), 1–9.

Al-Kdasi, A., Idris, A., Saed, K., & Guan, C. T. (2004). Treatment of textile wastewater by advanced oxidation processes– A review. *Global Nest Journal*, *6*(1), 222–230.

Anwer, H., Mahmood, A., Lee, J., Kim, K. H., Park, J. W., & Yip, A. C. K. (2019). Photocatalysts for degradation of dyes in industrial effluents: Opportunities and challenges. *Nano Research*, *12*(5), 955–972. https://doi.org/10.1007/s12274-019-2287-0

Arifin, M. N., Rezaul Karim, K. M., Abdullah, H., & Khan, M. R. (2019). Synthesis of titania doped copper ferrite photocatalyst and its photoactivity towards methylene blue degradation under visible light irradiation. *Bulletin of Chemical Reaction Engineering &Amp; Catalysis*, *14*(1), 219–227. https://doi.org/10.9767/bcrec.14.1.3616.219-227

Asadzadeh-Khaneghah, S., Habibi-Yangjeh, A., Seifzadeh, D., Chand, H., & Krishnan, V. (2021). Visible-light-activated g-C3N4 nanosheet/carbon dot/FeOCl nanocomposites: Photodegradation of dye pollutants and tetracycline hydrochloride. *Colloids and Surfaces A: Physicochemical and Engineering Aspects*, *617*(February), 126424. https://doi.org/10.1016/j.colsurfa.2021.126424

Ata, S., Shaheen, I., Qurat-ul-Ayne, Ghafoor, S., Sultan, M., Majid, F., Bibi, I., & Iqbal, M. (2018). Graphene and silver decorated ZnO composite synthesis, characterization and photocatalytic activity evaluation. *Diamond and Related Materials*, *90*(September), 26–31. https://doi.org/10.1016/j.diamond.2018.09.015

Balasurya, S., Das, A., Alyousef, A. A., Alqasim, A., Almutairi, N., & Sudheer Khan, S. (2021). Facile synthesis of Bi2MoO6-Ag2MoO4 nanocomposite for the enhanced visible light photocatalytic removal of methylene blue and its antimicrobial application. *Journal of Molecular Liquids*, *337*, 116350. https://doi.org/10.1016/j.molliq.2021.116350

Benedek, J., Sebestyén, T. T., & Bartók, B. (2018). Evaluation of renewable energy sources in

peripheral areas and renewable energy-based rural development. *Renewable and Sustainable Energy Reviews*, *90*(April), 516–535. https://doi.org/10.1016/j.rser.2018.03.020

Bi, J., Wu, L., Li, J., Li, Z., Wang, X., & Fu, X. (2007). Simple solvothermal routes to synthesize nanocrystalline Bi2MoO6 photocatalysts with different morphologies. *Acta Materialia*, *55*(14), 4699–4705. https://doi.org/10.1016/j.actamat.2007.04.034

Chahar, D., Taneja, S., Bisht, S., Kesarwani, S., Thakur, P., Thakur, A., & Sharma, P. B. (2021). Photocatalytic activity of cobalt substituted zinc ferrite for the degradation of methylene blue dye under visible light irradiation. *Journal of Alloys and Compounds*, *851*, 156878. https://doi.org/10.1016/j.jallcom.2020.156878

Chankhanittha, T., Somaudon, V., Watcharakitti, J., Piyavarakorn, V., & Nanan, S. (2020). Performance of solvothermally grown Bi2MoO6 photocatalyst toward degradation of organic azo dyes and fluoroquinolone antibiotics. *Materials Letters*, *258*, 126764. https://doi.org/10.1016/j.matlet.2019.126764

Chaudhary, K., Shaheen, N., Zulfiqar, S., Sarwar, M. I., Suleman, M., Agboola, P. O., Shakir, I., & Warsi, M. F. (2020). Binary WO3-ZnO nanostructures supported rGO ternary nanocomposite for visible light driven photocatalytic degradation of methylene blue. *Synthetic Metals*, *269*(May). https://doi.org/10.1016/j.synthmet.2020.116526

Chen, S., Hu, Y., Meng, S., & Fu, X. (2014). Study on the separation mechanisms of photogenerated electrons and holes for composite photocatalysts g-C3N4-WO3. *Applied Catalysis B: Environmental*, *150–151*, 564–573. https://doi.org/10.1016/j.apcatb.2013.12.053

Crini, G. (2006). Non-conventional low-cost adsorbents for dye removal: A review. *Bioresource Technology*, *97*(9), 1061–1085. https://doi.org/10.1016/j.biortech.2005.05.001

Dalvand, A., Gholami, M., Joneidi, A., & Mahmoodi, N. M. (2011). Dye Removal, Energy Consumption and Operating Cost of Electrocoagulation of Textile Wastewater as a Clean Process. *Clean - Soil, Air, Water*, *39*(7), 665–672. https://doi.org/10.1002/clen.201000233

Daneshvar, N., Ayazloo, M., Khataee, A. R., & Pourhassan, M. (2007). Biological

decolourization of dye solution containing Malachite Green by microalgae Cosmarium sp. *Bioresource Technology*, *98*(6), 1176–1182. https://doi.org/10.1016/j.biortech.2006.05.025

Deb, B., & Ghosh, A. (2011). Silver ion dynamics in Ag2S-doped silver molybdate-glass nanocomposites: Correlation of conductivity and scaling with structure. *Journal of Physical Chemistry C*, *115*(29), 14141–14147. https://doi.org/10.1021/jp204474n

Ding, J., Xu, W., Wan, H., Yuan, D., Chen, C., Wang, L., Guan, G., & Dai, W. L. (2018). Nitrogen vacancy engineered graphitic C3N4-based polymers for photocatalytic oxidation of aromatic alcohols to aldehydes. *Applied Catalysis B: Environmental*, *221*(September 2017), 626–634. https://doi.org/10.1016/j.apcatb.2017.09.048

El-Katori, E. E., Ahmed, M. A., El-Bindary, A. A., & Oraby, A. M. (2020). Impact of CdS/SnO2heterostructured nanoparticle as visible light active photocatalyst for the removal methylene blue dye. *Journal of Photochemistry and Photobiology A: Chemistry*, *392*(May 2019), 112403. https://doi.org/10.1016/j.jphotochem.2020.112403

El Qada, E. N., Allen, S. J., & Walker, G. M. (2008). Adsorption of basic dyes from aqueous solution onto activated carbons. *Chemical Engineering Journal*, *135*(3), 174–184. https://doi.org/10.1016/j.cej.2007.02.023

Eren, M. S. A., Arslanoglu, H., & Çiftçi, H. (2020). Production of microporous Cu-doped BTC (Cu-BTC) metal-organic framework composite materials, superior adsorbents for the removal of methylene blue (Basic Blue 9). *Journal of Environmental Chemical Engineering*, *8*(5). https://doi.org/10.1016/j.jece.2020.104247

Ferreira, W. H., Silva, L. G. A., Pereira, B. C. S., Gouvêa, R. F., & Andrade, C. T. (2020). Adsorption and visible-light photocatalytic performance of a graphene derivative for methylene blue degradation. *Environmental Nanotechnology, Monitoring and Management*, *14*(September), 23–26. https://doi.org/10.1016/j.enmm.2020.100373

Fu, H., Zhang, L., Yao, W., & Zhu, Y. (2006). Photocatalytic properties of nanosized Bi2WO6 catalysts synthesized via a hydrothermal process. *Applied Catalysis B: Environmental*, *66*(1–2), 100–110. https://doi.org/10.1016/j.apcatb.2006.02.022

Gao, L., Du, J., & Ma, T. (2017). Cysteine-assisted synthesis of CuS-TiO2 composites with enhanced photocatalytic activity. *Ceramics International*, *43*(12), 9559–9563. https://doi.org/10.1016/j.ceramint.2017.04.093

Ghattavi, S., & Nezamzadeh-Ejhieh, A. (2021). A double-Z-scheme ZnO/AgI/WO3 photocatalyst with high visible light activity: Experimental design and mechanism pathway in the degradation of methylene blue. *Journal of Molecular Liquids*, *322*(xxxx), 114563. https://doi.org/10.1016/j.molliq.2020.114563

Ghosh, U., & Pal, A. (2020). Fabrication of a novel Bi2O3 nanoparticle impregnated nitrogen vacant 2D g-C3N4 nanosheet Z scheme photocatalyst for improved degradation of methylene blue dye under LED light illumination. *Applied Surface Science*, *507*, 144965. https://doi.org/10.1016/j.apsusc.2019.144965

Goud, B. S., Koyyada, G., Jung, J. H., Reddy, G. R., Shim, J., Nam, N. D., & Vattikuti, S. V. P. (2020). Surface oxygen vacancy facilitated Z-scheme MoS2/Bi2O3 heterojunction for enhanced visible-light driven photocatalysis-pollutant degradation and hydrogen production. *International Journal of Hydrogen Energy*, *45*(38), 18961–18975. https://doi.org/10.1016/j.ijhydene.2020.05.073

Gouveia, A. F., Sczancoski, J. C., Ferrer, M. M., Lima, A. S., Santos, M. R. M. C., Li, M. S., Santos, R. S., Longo, E., & Cavalcante, L. S. (2014). Experimental and theoretical investigations of electronic structure and photoluminescence properties of β-Ag2MoO4 microcrystals. *Inorganic Chemistry*, *53*(11), 5589–5599. https://doi.org/10.1021/ic500335x

Guo, F., Shi, W., Lin, X., & Che, G. (2014). Hydrothermal synthesis of graphitic carbon nitride-BiVO4 composites with enhanced visible light photocatalytic activities and the mechanism study. *Journal of Physics and Chemistry of Solids*, *75*(11), 1217–1222. https://doi.org/10.1016/j.jpcs.2014.05.011

He, Y., Wang, Y., Zhang, L., Teng, B., & Fan, M. (2014). A new application of Z-Schene Ag_3PO_4/g-C_3N_4 composite in converting CO2 to fuel. *Environmental Science & Technology*.

Hong, Y., Jiang, Y., Li, C., Fan, W., Yan, X., Yan, M., & Shi, W. (2016). In-situ synthesis of

direct solid-state Z-scheme V2O5/g-C3N4 heterojunctions with enhanced visible light efficiency in photocatalytic degradation of pollutants. *Applied Catalysis B: Environmental*, *180*, 663–673. https://doi.org/10.1016/j.apcatb.2015.06.057

Hong, Y., Li, C., Zhang, G., Meng, Y., Yin, B., Zhao, Y., & Shi, W. (2016). Efficient and stable Nb2O5 modified g-C3N4 photocatalyst for removal of antibiotic pollutant. *Chemical Engineering Journal*, *299*, 74–84. https://doi.org/10.1016/j.cej.2016.04.092

Huang, Y., Li, H., Balogun, M. S., Liu, W., Tong, Y., Lu, X., & Ji, H. (2014). Oxygen vacancy induced bismuth oxyiodide with remarkably increased visible-light absorption and superior photocatalytic performance. *ACS Applied Materials and Interfaces*, *6*(24), 22920–22927. https://doi.org/10.1021/am507641k

Huang, Z., Jia, S., Wei, J., & Shao, Z. (2021). A visible light active, carbon-nitrogen-sulfur co-doped TiO2/g-C3N4Z-scheme heterojunction as an effective photocatalyst to remove dye pollutants. *RSC Advances*, *11*(27), 16747–16754. https://doi.org/10.1039/d1ra01890f

Imran, M., Crowley, D. E., Khalid, A., Hussain, S., Mumtaz, M. W., & Arshad, M. (2015). Microbial biotechnology for decolourization of textile wastewaters. *Reviews in Environmental Science and Biotechnology*, *14*(1), 73–92. https://doi.org/10.1007/s11157-014-9344-4

Iqbal, M., Bhatti, H. N., Younis, S., Rehmat, S., Alwadai, N., Almuqrin, A. H., & Iqbal, M. (2021). Graphene oxide nanocomposite with CuSe and photocatalytic removal of methyl green dye under visible light irradiation. *Diamond and Related Materials*, *113*(August 2020), 108254. https://doi.org/10.1016/j.diamond.2021.108254

Jana, A., & Gregory, D. H. (2020). Microwave-Assisted Synthesis of ZnO–rGO Core–Shell Nanorod Hybrids with Photo- and Electro-Catalytic Activity. *Chemistry - A European Journal*, *26*(29), 6703–6714. https://doi.org/10.1002/chem.202000535

Khan, M. E., Khan, M. M., & Cho, M. H. (2017). Ce3+-ion, Surface Oxygen Vacancy, and Visible Light-induced Photocatalytic Dye Degradation and Photocapacitive Performance of CeO2-Graphene Nanostructures. *Scientific Reports*, *7*(1), 1–17. https://doi.org/10.1038/s41598-017-06139-6

Kos, L. (2016). Use of chitosan for textile wastewater decolourization. *Fibres and Textiles in Eastern Europe*, *24*(3), 130–135. https://doi.org/10.5604/12303666.1196623

Kumar, S., Kumar, B., Baruah, A., & Shanker, V. (2013). *S. Kumar, S. T, B. Kumar, A. Baruah, and V. Shanker, "Synthesis of Magnetically Separable and Recyclable g-C3N4–Fe3O4 Hybrid Nanocomposites with Enhanced Photocatalytic Performance under Visible-Light Irradiation," The Journal of Physical Chemistry C, vol*.

La Cruz, A. M. De, & Lozano, L. G. G. (2010). Photoassisted degradation of organic dyes by β-Bi2Mo 2O9. *Reaction Kinetics, Mechanisms and Catalysis*, *99*(1), 209–215. https://doi.org/10.1007/s11144-009-0112-3

Lei, Y., Ding, J., Yu, P., He, G., Chen, Y., & Chen, H. (2020). Low-temperature preparation of magnetically separable Fe3O4@ZnO-RGO for high-performance removal of methylene blue in visible light. *Journal of Alloys and Compounds*, *821*, 153366. https://doi.org/10.1016/j.jallcom.2019.153366

Li, Haijin, Zhou, Y., Tu, W., Ye, J., & Zou, Z. (2015). State-of-the-art progress in diverse heterostructured photocatalysts toward promoting photocatalytic performance. *Advanced Functional Materials*, *25*(7), 998–1013. https://doi.org/10.1002/adfm.201401636

Li, Honghua, Liu, C., Li, K., & Wang, H. (2008). Preparation, characterization and photocatalytic properties of nanoplate Bi2MoO6 catalysts. *Journal of Materials Science*, *43*(22), 7026–7034. https://doi.org/10.1007/s10853-008-3034-y

Li, S., Xue, B., Wang, C., Jiang, W., Hu, S., Liu, Y., Wang, H., & Liu, J. (2019). Facile fabrication of flower-like BiOI/BiOCOOH p–n heterojunctions for highly efficient visible-light-driven photocatalytic removal of harmful antibiotics. *Nanomaterials*, *9*(11), 1–14. https://doi.org/10.3390/nano9111571

Liu, J., Liu, Y., Liu, N., Han, Y., Zhang, X., Huang, H., Lifshitz, Y., Lee, S., Zhong, J., & Kang, Z. (2015). *R es e a rc h | r e po r ts*. *0006709*(i), 1–6.

Liu, X., Jin, A., Jia, Y., Xia, T., Deng, C., Zhu, M., Chen, C., & Chen, X. (2017). Synergy of adsorption and visible-light photocatalytic degradation of methylene blue by a bifunctional

Z-scheme heterojunction of WO 3 /g-C 3 N 4. *Applied Surface Science*, *405*, 359–371. https://doi.org/10.1016/j.apsusc.2017.02.025

Lou, X. W., & Zeng, H. C. (2003). An inorganic route for controlled synthesis of W18O 49 nanorods and nanofibers in solution. *Inorganic Chemistry*, *42*(20), 6169–6171. https://doi.org/10.1021/ic034771q

Ma, L., Jia, I., Guo, X., & Xiang, L. (2014). High performance of Pd catalysts on bimodal mesopore for the silica catalytic oxidation of toluene. *Chinese Journal of Catalysis*, *35*(0), 108–119. https://doi.org/10.1016/S1872

Ma, Y., Chen, Y., Feng, Z., Zeng, L., Chen, Q., Jin, R., Lu, Y., Huang, Y., Wu, Y., & He, Y. (2017). Preparation, characterization of Bi3O4Cl/g-C3N4 composite and its photocatalytic activity in dye degradation. *Journal of Water Process Engineering*, *18*(March), 65–72. https://doi.org/10.1016/j.jwpe.2017.06.002

Majumdar, A., Ghosh, U., & Pal, A. (2021). Novel 2D/2D g-C3N4/Bi4NbO8Cl nano-composite for enhanced photocatalytic degradation of oxytetracycline under visible LED light irradiation. *Journal of Colloid and Interface Science*, *584*, 320–331. https://doi.org/10.1016/j.jcis.2020.09.101

Majumdar, A., & Pal, A. (2020). Recent advancements in visible-light-assisted photocatalytic removal of aqueous pharmaceutical pollutants. In *Clean Technologies and Environmental Policy* (Vol. 22, Issue 1). Springer Berlin Heidelberg. https://doi.org/10.1007/s10098-019-01766-1

Mao, W., Zhang, L., Wang, T., Bai, Y., & Guan, Y. (2021). Fabrication of highly efficient Bi2WO6/CuS composite for visible-light photocatalytic removal of organic pollutants and Cr(VI) from wastewater. *Frontiers of Environmental Science and Engineering*, *15*(4). https://doi.org/10.1007/s11783-020-1344-8

Martínez-de la Cruz, A., & Obregón Alfaro, S. (2010). Synthesis and characterization of γ-Bi2MoO6 prepared by co-precipitation: Photoassisted degradation of organic dyes under vis-irradiation. *Journal of Molecular Catalysis A: Chemical*, *320*(1–2), 85–91. https://doi.org/10.1016/j.molcata.2010.01.008

Meng, Z., & Juan, Z. (2008). Wastewater treatment by photocatalytic oxidation of Nano-ZnO 2 principles of photocatalytic oxidation (Cui (2001), Lei (2001)) Synthesization of Nano-ZnO. *Science*, *12*(12), 1–9.

Mohamad Idris, N. H., Rajakumar, J., Cheong, K. Y., Kennedy, B. J., Ohno, T., Yamakata, A., & Lee, H. L. (2021). Titanium Dioxide/Polyvinyl Alcohol/Cork Nanocomposite: A Floating Photocatalyst for the Degradation of Methylene Blue under Irradiation of a Visible Light Source. *ACS Omega*. https://doi.org/10.1021/acsomega.1c01458

Mohamed, R. M., McKinney, D. L., & Sigmund, W. M. (2012). Enhanced nanocatalysts. *Materials Science and Engineering R: Reports*, *73*(1), 1–13. https://doi.org/10.1016/j.mser.2011.09.001

Mohan, D., Singh, K. P., Singh, G., & Kumar, K. (2002). Removal of dyes from wastewater using flyash, a low-cost adsorbent. *Industrial and Engineering Chemistry Research*, *41*(15), 3688–3695. https://doi.org/10.1021/ie010667+

Mokif, L. A. (2019). Removal Methods of Synthetic Dyes from Industrial Wastewater: A review. *Mesopo. Environ. J*, *5*(1), 23–40. http//:www.bumej.com

Mosavi, S. A., Ghadi, A., Gharbani, P., & Mehrizad, A. (2021). Photocatalytic removal of Methylene Blue using Ag@CdSe/Zeoilte nanocomposite under visible light irradiation by Response Surface Methodology. *Materials Chemistry and Physics*, *267*(November 2020), 124696. https://doi.org/10.1016/j.matchemphys.2021.124696

Natarajan, T. S., Thampi, K. R., & Tayade, R. J. (2018). Visible light driven redox-mediator-free dual semiconductor photocatalytic systems for pollutant degradation and the ambiguity in applying Z-scheme concept. *Applied Catalysis B: Environmental*, *227*, 296–311. https://doi.org/10.1016/j.apcatb.2018.01.015

Niu, P., Qiao, M., Li, Y., Huang, L., & Zhai, T. (2018). Distinctive defects engineering in graphitic carbon nitride for greatly extended visible light photocatalytic hydrogen evolution. *Nano Energy*, *44*, 73–81. https://doi.org/10.1016/j.nanoen.2017.11.059

Niu, P., Zhang, L., Liu, G., & Cheng, H. M. (2012). Graphene-like carbon nitride nanosheets for

improved photocatalytic activities. *Advanced Functional Materials*, *22*(22), 4763–4770. https://doi.org/10.1002/adfm.201200922

Noman, A. M. A., Alghobar, M. A., & Suresha, S. (2021). Synthesis and activity evaluation of p-n CuO/CeO2-ZrO2 heterojunction photocatalyst for the removal of dye from industrial wastewater under visible light irradiation. *Journal of Water and Environmental Nanotechnology*, *6*(1), 1–10. https://doi.org/10.22090/jwent.2021.01.001

Opoku, F., Govender, K. K., Sittert, C. G. C. E. van, & Govender, P. P. (2018). Insights into the photocatalytic mechanism of mediator-free direct Z-scheme g-C 3 N 4 /Bi 2 MoO 6 (010) and g-C 3 N 4 /Bi 2 WO 6 (010) heterostructures: A hybrid density functional theory study. *Applied Surface Science*, *427*, 487–498. https://doi.org/10.1016/j.apsusc.2017.09.019

Ou, H., Lin, L., Zheng, Y., Yang, P., Fang, Y., & Wang, X. (2017). Tri-s-triazine-Based Crystalline Carbon Nitride Nanosheets for an Improved Hydrogen Evolution. *Advanced Materials*, *29*(22). https://doi.org/10.1002/adma.201700008

Panneri, S., Ganguly, P., Mohan, M., Nair, B. N., Mohamed, A. A. P., Warrier, K. G., & Hareesh, U. S. (2017). Photoregenerable, bifunctional granules of carbon-doped g-C3N4 as adsorptive photocatalyst for the efficient removal of tetracycline antibiotic. *ACS Sustainable Chemistry and Engineering*, *5*(2), 1610–1618. https://doi.org/10.1021/acssuschemeng.6b02383

Paquin, F., Rivnay, J., Salleo, A., Stingelin, N., & Silva, C. (2015). Multi-phase semicrystalline microstructures drive exciton dissociation in neat plastic semiconductors. *J. Mater. Chem. C*, *3*(207890), 10715–10722. https://doi.org/10.1039/b000000x

Pelaez, M., Nolan, N. T., Pillai, S. C., Seery, M. K., Falaras, P., Kontos, A. G., Dunlop, P. S. M., Hamilton, J. W. J., Byrne, J. A., O'Shea, K., Entezari, M. H., & Dionysiou, D. D. (2012). A review on the visible light active titanium dioxide photocatalysts for environmental applications. *Applied Catalysis B: Environmental*, *125*, 331–349. https://doi.org/10.1016/j.apcatb.2012.05.036

Phuruangrat, A., Jitrou, P., Dumrongrojthanath, P., Ekthammathat, N., Kuntalue, B., Thongtem, S., & Thongtem, T. (2013). Hydrothermal synthesis and characterization of Bi2MoO 6

nanoplates and their photocatalytic activities. *Journal of Nanomaterials*, *2013*. https://doi.org/10.1155/2013/789705

Potti, P. R., & Srivastava, V. C. (2013). Effect of dopants on Zno mediated photocatalysis of dye bearing wastewater: A review. *Materials Science Forum*, *757*, 165–174. https://doi.org/10.4028/www.scientific.net/MSF.757.165

Prabakaran, E., & Pillay, K. (2019). Synthesis of N-doped ZnO nanoparticles with cabbage morphology as a catalyst for the efficient photocatalytic degradation of methylene blue under UV and visible light. *RSC Advances*, *9*(13), 7509–7535. https://doi.org/10.1039/C8RA09962F

Pruden, A. L., & Ollis, D. F. (1983). Photoassisted heterogeneous catalysis: The degradation of trichloroethylene in water. *Journal of Catalysis*, *82*(2), 404–417. https://doi.org/10.1016/0021-9517(83)90207-5

Sá, J., Fernández-García, M., & Anderson, J. A. (2008). Photoformed electron transfer from TiO2 to metal clusters. *Catalysis Communications*, *9*(10), 1991–1995. https://doi.org/10.1016/j.catcom.2008.03.041

Shen, S., Guo, L., Chen, X., Ren, F., Kronawitter, C. X., & Mao, S. S. (2010). Effect of Noble Metal in CdS/M/TiO 2 for Photocatalytic Degradation of Methylene Blue under Visible Light. *International Journal of Green Nanotechnology: Materials Science and Engineering*, *1*(2), 37–41. https://doi.org/10.1080/19430841003684823

Shi, L., Liang, L., Ma, J., Meng, Y., Zhong, S., Wang, F., & Sun, J. (2014). Highly efficient visible light-driven Ag/AgBr/ZnO composite photocatalyst for degrading Rhodamine B. *Ceramics International*, *40*(2), 3495–3502. https://doi.org/10.1016/j.ceramint.2013.09.080

Shinde, S. S., Bhosale, C. H., & Rajpure, K. Y. (2012). Photocatalytic degradation of toluene using sprayed N-doped ZnO thin films in aqueous suspension. *Journal of Photochemistry and Photobiology B: Biology*, *113*, 70–77. https://doi.org/10.1016/j.jphotobiol.2012.05.008

Sun, S., Chang, X., Li, X., & Li, Z. (2013). Synthesis of N-doped ZnO nanoparticles with improved photocatalytical activity. *Ceramics International*, *39*(5), 5197–5203.

https://doi.org/10.1016/j.ceramint.2012.12.018

Sun, Y., Wang, W., Zhang, L., & Sun, S. (2013). The photocatalysis of Bi2MoO6 under the irradiation of blue LED. *Materials Research Bulletin*, *48*(10), 4357–4361. https://doi.org/10.1016/j.materresbull.2013.07.015

Tian, G., Chen, Y., Zhou, W., Pan, K., Dong, Y., Tian, C., & Fu, H. (2011). Facile solvothermal synthesis of hierarchical flower-like Bi2MoO6 hollow spheres as high performance visible-light driven photocatalysts. *Journal of Materials Chemistry*, *21*(3), 887–892. https://doi.org/10.1039/c0jm03040f

Tokunaga, S., Kato, H., & Kudo, A. (2001). Selective preparation of monoclinic and tetragonal BiVO4 with scheelite structure and their photocatalytic properties. *Chemistry of Materials*, *13*(12), 4624–4628. https://doi.org/10.1021/cm0103390

Viswanathan, B. (2017). Photocatalytic Degradation of Dyes: An Overview. *Current Catalysis*, *7*(2), 99–121. https://doi.org/10.2174/2211544707666171219161846

Wahlström, N., Steinhagen, S., Toth, G., Pavia, H., & Edlund, U. (2020). Ulvan dialdehyde-gelatin hydrogels for removal of heavy metals and methylene blue from aqueous solution. *Carbohydrate Polymers*, *249*(July 2020). https://doi.org/10.1016/j.carbpol.2020.116841

Wang, M., Tan, G., Zhang, D., Li, B., Lv, L., Wang, Y., Ren, H., Zhang, X. L., Xia, A., & Liu, Y. (2019). Defect-mediated Z-scheme BiO2-x/Bi2O2.75 photocatalyst for full spectrum solar-driven organic dyes degradation. *Applied Catalysis B: Environmental*, *254*(April), 98–112. https://doi.org/10.1016/j.apcatb.2019.04.044

Xie, H., Shen, D., Wang, X., & Shen, G. (2007). Microwave hydrothermal synthesis and visible-light photocatalytic activity of Bi2WO6 nanoplates. *Materials Chemistry and Physics*, *103*(2–3), 334–339. https://doi.org/10.1016/j.matchemphys.2007.02.040

Xie, L., Ma, J., & Xu, G. (2008). Preparation of a novel Bi2MoO6 flake-like nanophotocatalyst by molten salt method and evaluation for photocatalytic decomposition of rhodamine B. *Materials Chemistry and Physics*, *110*(2–3), 197–200. https://doi.org/10.1016/j.matchemphys.2008.01.035

Xing, C., Wu, Z., Jiang, D., & Chen, M. (2014). Hydrothermal synthesis of In2S3/g-C3N4 heterojunctions with enhanced photocatalytic activity. *Journal of Colloid and Interface Science*, *433*, 9–15. https://doi.org/10.1016/j.jcis.2014.07.015

Xu, G., Zhang, H., Wei, J., Zhang, H. X., Wu, X., Li, Y., Li, C., Zhang, J., & Ye, J. (2018). Integrating the g-C3N4 Nanosheet with B-H Bonding Decorated Metal-Organic Framework for CO2 Activation and Photoreduction. *ACS Nano*, *12*(6), 5333–5340. https://doi.org/10.1021/acsnano.8b00110

Xu, Q., Zhang, L., Yu, J., Wageh, S., Al-Ghamdi, A. A., & Jaroniec, M. (2018). Direct Z-scheme photocatalysts: Principles, synthesis, and applications. *Materials Today*, *21*(10), 1042–1063. https://doi.org/10.1016/j.mattod.2018.04.008

Xue, J., Ma, S., Zhou, Y., Zhang, Z., & He, M. (2015). Facile photochemical synthesis of Au/Pt/g-C3N4 with plasmon-enhanced photocatalytic activity for antibiotic degradation. *ACS Applied Materials and Interfaces*, *7*(18), 9630–9637. https://doi.org/10.1021/acsami.5b01212

Yan, C., & Liu, L. (2020). Sn-doped V2O5 nanoparticles as catalyst for fast removal of ammonia in air via PEC and PEC-MFC. *Chemical Engineering Journal*, *392*, 123738. https://doi.org/10.1016/j.cej.2019.123738

Yang, G., Liang, Y., Li, K., Yang, J., Wang, K., Xu, R., & Xie, X. (2020). Engineering the dimension and crystal structure of bismuth molybdate photocatalysts via a molten salt-assisted assembly approach. *Journal of Alloys and Compounds*, *844*, 156231. https://doi.org/10.1016/j.jallcom.2020.156231

Yang, J., Jing, R., Wang, P., Liang, D. R., Huang, H., Xia, C., Zhang, Q., Liu, A., Meng, Z., & Liu, Y. (2021). Black phosphorus nanosheets and ZnAl-LDH nanocomposite as environmental-friendly photocatalysts for the degradation of Methylene blue under visible light irradiation. *Applied Clay Science*, *200*(September), 105902. https://doi.org/10.1016/j.clay.2020.105902

Yang, P., Ou, H., Fang, Y., & Wang, X. (2017). A Facile Steam Reforming Strategy to Delaminate Layered Carbon Nitride Semiconductors for Photoredox Catalysis. *Angewandte*

Chemie, *129*(14), 4050–4054. https://doi.org/10.1002/ange.201700286

Yin, W., Wang, W., & Sun, S. (2010). Photocatalytic degradation of phenol over cage-like Bi2MoO6 hollow spheres under visible-light irradiation. *Catalysis Communications*, *11*(7), 647–650. https://doi.org/10.1016/j.catcom.2010.01.014

Zhang, D. (2012). Visible light-induced photocatalysis through surface plasmon excitation of platinum-metallized titania for photocatalytic bleaching of rhodamine B. *Monatshefte Fur Chemie*, *143*(5), 729–738. https://doi.org/10.1007/s00706-011-0631-2

Zhang, J., Hu, Y., Jiang, X., Chen, S., Meng, S., & Fu, X. (2014). Design of a direct Z-scheme photocatalyst: Preparation and characterization of Bi2O3/g-C3N4 with high visible light activity. *Journal of Hazardous Materials*, *280*, 713–722. https://doi.org/10.1016/j.jhazmat.2014.08.055

Zhang, Xiaodong, Xie, X., Wang, H., Zhang, J., Pan, B., & Xie, Y. (2013). Enhanced photoresponsive ultrathin graphitic-phase C3N 4 nanosheets for bioimaging. *Journal of the American Chemical Society*, *135*(1), 18–21. https://doi.org/10.1021/ja308249k

Zhang, Xinfei, Jia, X., Duan, P., Xia, R., Zhang, N., Cheng, B., Wang, Z., & Zhang, Y. (2021). V2O5/P-g-C3N4 Z-scheme enhanced heterogeneous photocatalytic removal of methyl orange from water under visible light irradiation. *Colloids and Surfaces A: Physicochemical and Engineering Aspects*, *608*(July 2020), 125580. https://doi.org/10.1016/j.colsurfa.2020.125580

Zhang, Y., Chen, Z., Shi, Z., Lu, T., Chen, D., Wang, Q., & Zhan, Z. (2021). A direct Z-scheme BiOBr/TzDa COF heterojunction photocatalyst with enhanced performance on visible-light driven removal of organic dye and Cr(VI). *Separation and Purification Technology*, *275*(June), 119216. https://doi.org/10.1016/j.seppur.2021.119216

Zhang, Z., Zhao, C., Lin, S., Li, H., Feng, Y., & Gao, X. (2021). Oxygen vacancy modified Bi2MoO6/WO3 electrode with enhanced photoelectrocatalytic degradation activity toward RhB. *Fuel*, *285*(August 2020), 119171. https://doi.org/10.1016/j.fuel.2020.119171

Zhao, Xiaohua, Li, M., & Lou, X. (2014). Sol-gel assisted hydrothermal synthesis of ZnO

microstructures: Morphology control and photocatalytic activity. *Advanced Powder Technology*, *25*(1), 372–378. https://doi.org/10.1016/j.apt.2013.06.004

Zhao, Xu, Qu, J., Liu, H., & Hu, C. (2007). Photoelectrocatalytic degradation of triazine-containing azo dyes at γ-Bi2MoO6 film electrode under visible light irradiation (λ > 420 Nm). *Environmental Science and Technology*, *41*(19), 6802–6807. https://doi.org/10.1021/es070598b

Zhao, Xu, Xu, T., Yao, W., & Zhu, Y. (2009). Photodegradation of dye pollutants catalyzed by γ-Bi 2 MoO 6 nanoplate under visible light irradiation. *Applied Surface Science*, *255*(18), 8036–8040. https://doi.org/10.1016/j.apsusc.2009.05.010

Zhong, W., Lou, Y., Jin, S., Wang, W., & Guo, L. (2016). A new Bi-based visible-light-sensitive photocatalyst BiLa1.4Ca0.6O4.2: Crystal structure, optical property and photocatalytic activity. *Scientific Reports*, *6*(March), 1–7. https://doi.org/10.1038/srep23235

Zhou, L., Wang, W., & Zhang, L. (2007). Ultrasonic-assisted synthesis of visible-light-induced Bi2MO6 (M = W, Mo) photocatalysts. *Journal of Molecular Catalysis A: Chemical*, *268*(1–2), 195–200. https://doi.org/10.1016/j.molcata.2006.12.026

Zhu, B., Xia, P., Ho, W., & Yu, J. (2015). Isoelectric point and adsorption activity of porous g-C 3 N 4. *Applied Surface Science*, *344*, 188–195. https://doi.org/10.1016/j.apsusc.2015.03.086

Zhu, Y. N., Mu, J. J., Zheng, G. H., Dai, Z. X., Zhang, L. Y., Ma, Y. Q., & Zhang, D. W. (2016). Morphology, photocatalytic and photoelectric properties of Bi2MoO6 tuned by preparation method, solvent, and surfactant. *Ceramics International*, *42*(15), 17347–17356. https://doi.org/10.1016/j.ceramint.2016.08.031

Zhu, Z., Mankowski, T., Balakrishnan, K., Shikoh, A. S., Touati, F., Benammar, M. A., Mansuripur, M., & Falco, C. M. (2015). Ultrahigh Aspect Ratio Copper-Nanowire-Based Hybrid Transparent Conductive Electrodes with PEDOT:PSS and Reduced Graphene Oxide Exhibiting Reduced Surface Roughness and Improved Stability. *ACS Applied Materials and Interfaces*, *7*(30), 16223–16230. https://doi.org/10.1021/acsami.5b01379